Topological Analysis of Pore and Contact Networks

A Thesis

submitted to
Indian Institute of Science Education and Research Pune
in partial fulfillment of the requirements for the
BS-MS Dual Degree Programme

by

Heerak Sharma

Indian Institute of Science Education and Research Pune
Dr. Homi Bhabha Road,
Pashan, Pune 411008, INDIA.

May, 2026

Supervisor: Vijay Natarajan

Certificate

This is to certify that this dissertation entitled Topological Analysis of Pore and Contact Networks towards the partial fulfilment of the BS-MS dual degree programme at the Indian Institute of Science Education and Research, Pune represents study/work carried out by Heerak Sharma at Indian Institute of Science, Bangalore under the supervision of Vijay Natarajan, Professor, Department of Computer Science and Automation, during the academic year 2025-2026.

Vijay Natarajan

Committee:

Vijay Natarajan

Rama Mishra

This thesis is dedicated to the few good people in Indian healthcare who actually care about their patients.

Declaration

I hereby declare that the matter embodied in the report entitled Topological Analysis of Pore and Contact Networks are the results of the work carried out by me at Visualization and Graphics lab, Department of Computer Science and Automation, Indian Institute of Science, Bangalore, under the supervision of Prof. Vijay Natarajan and the same has not been submitted elsewhere for any other degree.

Heerak Sharma

Acknowledgments

I express my deepest gratitude to my supervisor Prof. Vijay Natarajan not only for his guidance, discussions and insights but also for his kindness, understanding and unwavering support throughout my thesis. His way of thinking especially his intuition has left a positive, lasting impact on my way of approaching problems. I would also like to thank Prof. Rama Mishra for being the expert member for my thesis. I am also grateful to Vishali S, Prof. Tejas Kalelkar and Dr. Udayan Kanade for the valuable insights I gained from my discussions with them.

I thank my family – my mom Mrs. Shakuntla Sharma; my dad Mr. Moti Lal Sharma; my sister Mrs. Komal Sharma; and brother in law Mr. Sandeep Sharma for their constant support. Even in tough times, they kept my study on high priority. I also want to thank my extended family members – Mr. Vikram Jangid, Mrs. Sarita Jangid, Mr. Hitesh Jangid, Mr. Manoj Jangid, Mrs. Suman Jangid and Mrs. Kanchan Jangid. My counsellor, Dipika Khandelval, helped me understand myself during this thesis. My friends – Chitvan Singh, Praneet Kumar Patra and Ipsa Bezbarua have always been there for me.

I would also thank Dr. Asha Kapadia, Dr. Navroz Mehta, Dr. Renu Duhan, Dr. Satya Narayan Sarswat, Dr. Mohnish Grover, Dr. Manoj Jangid, Dr. Deepak Chabra PT, Dr. Charmi Kaushik PT for their support towards my parent's health.

Lastly, I would also thank the people who maintain resources like Wikipedia, n-Lab, stack exchange, YouTube channels and many more.

Abstract

Granular materials are composed of discrete macroscopic particles and the empty spaces, or voids, between them. While the physical and geometric properties of the particle space are extensively studied, the void space is equally critical for understanding macroscopic behaviors like permeability and mass transport but remains historically under-analyzed. This thesis explores the topological relationship between these two complementary spaces, ignoring their geometric complexity. We review robust, noise-resistant segmentation frameworks: Morsegram for Morse theory-based particle segmentation and Lovamap for medial axis-based void segmentation.

We explore the use of Alexander duality to relate homological features in the particle space to the homological features in the void space. We also explore the contact network and derive an expression of first Betti number of the particle space in terms of average coordination number of the material.

We also explore the use of handlebody theory and dual blocks in the context of granular materials.

Contents

Introduction

Granular materials, called granular because they consist of small particles that are packed together, comprise of a very important class of materials. These materials are ubiquitous – they span a great deal of nature for example, snow, sand, soil, concrete, industrial powders and mixtures, drug delivery systems, a jar of nuts, intergalactic dust, etc. The study of granular materials, therefore, spans a big collection of areas that include mathematics, physics, chemistry, earth science, pharmacology, bioengineering, manufacturing, and many more [12, 27, 24, 6].

Apart from the particles, a granular material naturally also consists of the empty spaces between the particles called the voids. Voids are inevitable, practically speaking, because no two particles are fit into each other perfectly without leaving any empty space around them. The collection (union) of all particles in a granular material is called the *particle space* and the collection (union) of all voids is called the *void space*. In order to understand granular materials, one needs to understand *both* particles and voids. There are many phenomena that depend more on the structure of the particle space, for example, force chains, shear response, and there are many other phenomena that depend more on the structure of the void space, for example, percolation, mass transport through the material. For a number of applications, void space metrics are more meaningful than particle space metrics. For example, in landslide and earthquake science, the voids are places that aid particle rearrangement and therefore contribute to instability.

The study of particles began well before Kepler who conjectured the optimal packing for spheres is the face centered cubic packing in 1611 [13]. In granular material's literature, a great deal of work studies the particle space but less attention has been paid to the voids even though both of them are equally important. This is because the particle space is easier to study because it consists of discrete objects where as the voids space, by definition is the

complement of the particle space, and is more continuous in some sense. For example, the connectivity of the particle space can be captured in a graph called the *contact network* that has a vertex for each particle in the granular material and an edge between two vertices if the corresponding particles are in contact with each other. Defining an analogous void network is harder because there is not a canonical segmentation of the voids in contrast to the particles.

One way to study granular materials is to study their X-ray CT scans. This is a non-invasive way to look inside the granular materials. This comes with a cost, the CT scan forgets where the individual particles are and they need to be segmented. In this thesis, we discuss *Morsegram* [23] which is a framework that uses the Morse complex to carry out particle segmentation. Void segmentation is the naturally the next thing to do and we discuss *Lovamap* [25], a clever medial axis based framework that segments the voids in a meaningful manner.

It is obvious that geometry of the particles in the particle space and the voids in the void space are of crucial importance. However, in this thesis, we ignore geometry in the situation like the shape and size of the particles, their orientation in space, etc and look at only the topology. Obviously the geometry is way more complicated than the topology. We primarily explore how complementary the particle space and the void space are from a topological perspective. To what extent can we infer the topology of one from the other? This is important because as have discussed, the particle space is easier to study than the void space and hence inferring something about the void space from the particle space is something useful. This is done mainly using Alexander duality, a famous result in Algebraic topology that relates the cohomology groups of a nice subset to the homology groups of its complement. We have also tried some computational experiments to see how well they work for granular materials. This is done in Chapter 3.

We also discuss results about the contact network and the void network. First, we also give a relation between the coordination numbers of the particles in the material and the first Betti numbers of the material. This is done by applying the first handshaking lemma to the contact network. Next, we discuss a relation between percolation threshold and persistence diagrams given by [26]. This is done in Chapter 4.

The outline of the thesis is as follows. Part I discusses the background and preliminaries for this thesis. It consists of Chapter 1, which discusses mathematical preliminaries and Chapter 2 which discussed granular materials background. Part II of the thesis discusses

the work done in the thesis. Chapter 3 explores the use of Alexander duality in granular materials. Chapter 4 explores some graph theoretic ideas. Chapter 5 discusses potential use of 1-handlebodies in granular materials, use of dual block decomposition, etc. Lastly, we end with Chapter 6 which is conclusions and future work.

Part I

Background and Preliminaries

Chapter 1

Mathematical Background

1.1 Basic Algebraic Topology

For basic algebraic topological notions such as homology, cohomology, fundamental groups, we refer to [11] and [20]. We introduce a notation for Betti numbers that we will follow in this thesis.

Let X be a topological space, then the kth Betti number of X will be denoted by $\beta_k(X)$.

Sometimes, classes in the homology groups will also be referred to as 'features'.

1.2 Nerve and Nerve Theorem

Let $\mathcal{I}$ be an indexing set. Let $\mathcal{A} = \{A_i \mid i \in \mathcal{I}\}$ be a family of subsets of a topological space X. The nerve of $\mathcal{A}$, denoted by $\mathcal{N}(\mathcal{A})$ is a simplicial complex with the vertex set $\mathcal{I}$ such that $\mathcal{J} \subset \mathcal{I}$ is a face if and only if $\cap_{j\in\mathcal{J}} A_j \neq \emptyset$.

We have a nice theorem due to Leray that states when the nerve $\mathcal{N}(\mathcal{A})$ is homotopy equivalent to the union of the family sets in $\mathcal{A}$.

Theorem 1.2.1. *Given a family of subsets $\mathcal{A} = \{A_i \mid i \in \mathcal{I}\}$. If for all finite subsets $\mathcal{J} \subset \mathcal{I}$, $\cap_{j\in\mathcal{J}} A_j$ is either empty or contractible, then $\mathcal{N}(\mathcal{A})$ is homotopy equivalent to $\cup_{i\in\mathcal{I}} A_i$.*

1.3 Morse theory

Morse theory is an attempt to understand the topology of a smooth manifold by studying real valued smooth functions on it. We first consider two classic examples 1) topographic altitude and 2) height function on a torus to understand the idea behind Morse theory.

1.3.1 Illustrative Example 1

Example 1. *Consider a geological terrain full of mountains and valleys. Assume that we live in a very idealized and smooth world such that our geological terrain is a smooth manifold M. The altitude is then a smooth function $f : M \to \mathbb{R}$. Consider the sub-level set $M_a = f^{-1}(-\infty, a]$ which is the set of all points in M with altitude less than or equal to a. Another way to think about M_a is that it is the part of M covered under water if we submerge the entire geological terrain M with water till altitude a.*

Notice that for different values of altitude a, the sets M_a can have different topology. The premise of Morse theory is that the altitudes a where the topology of M_a changes are critical points *of the altitude function f, points where the* gradient *of the altitude function vanishes. Following our submerged terrain example, the topology of M_a does not change except when the water*

1. *either starts filling a basin (valley),*

2. *covers a saddle (a mountain pass),*

3. *or submerges a peak (top of the mountain).*

To each of these three critical points, one associates a number called the *index*, which, informally speaking, is the number of independent directions at the critical point in which the altitude decreases. For basins, the index is 0, for saddles, the index is 1 and for peaks, the index is 2.

1.3.2 Illustrative Example 2

Another example from [7] is as follows. All of the figures in this example are taken from the Wikipedia article [32].

Example 2. *Let M be a torus as oriented as in the following figure.*

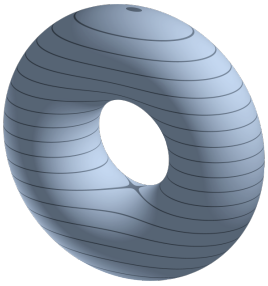

Figure 1.1: The torus M in discussion. It is like a doughnut kept upright on a table.

As before, we consider the height function of the torus $h : M \to \mathbb{R}$ mapping each point to its height. It is easy to see that the torus has four critical points p, q, r and s as described in the following figure. We define $M_a = h^{-1}(-\infty, a]$ as before.

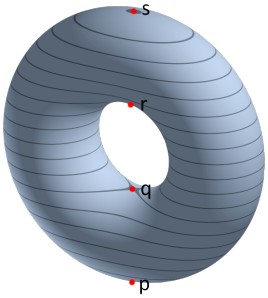

Figure 1.2: The four critical points p, q, r and s marked as red dots on the torus M. p is the lowest point of M, q and r are saddle points and s is the highest point in M.

The indices of these critical points are p, q, r and s are 0, $1, 1$ and 2 respectively. When $a < h(p)$, then M_a is the empty set. After a passes the level of p, when $f(p) < a < f(q)$ then M_a is a disk, which is homotopy equivalent to a point. Next, after a passes the level of q, when $f(q) < a < f(r)$, then M_a is homotopy equivalent to cylinder. Once a passes the level

of r, when $f(r) < a < f(s)$, then M_a is a torus with a disk removed. Finally, after a passes the level of s, $a \geq f(s)$, then M_a is the torus M itself. Please refer to the following figures.

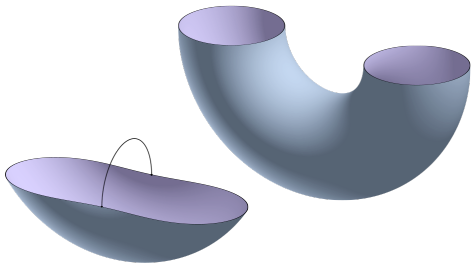

Figure 1.3: M_a is homotopy equivalent to a disc when $f(p) < a < f(q)$ and M_a is homotopy equivalent to a cylinder when $f(q) < a < f(r)$.

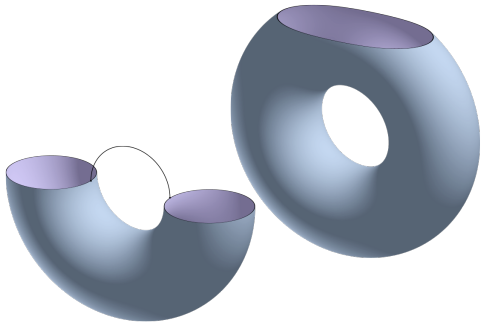

Figure 1.4: M_a is homotopy equivalent to a torus with a disc removed when $a \geq f(s)$ and M_a is homotopy equivalent to a cylinder with a 1-cell attached when $f(r) < a < f(s)$.

In general, the index of a non-degenerate critical point is defined to be the dimension of the largest (precisely, maximal subspace) subspace of the tangent space at the critical point on which the Hessian is negative definite. This corresponds to the intuitive notion that the index is the number of directions in which the function decreases. It follows from Sylvester's law of inertia that the degeneracy and index of a critical point are independent of the choice of the local coordinate system used.

Note that it is important that the critical points are non-degenerate, i. e., the Hessian at the critical points should not be zero.

1.3.3 Definitions

Now that the idea is clear from the above examples, we will define everything rigorously. We follow [17] in this and the also in next section but to a lesser extent.

Definition 1.3.1. *Let M be a smooth n-manifold and $f : M \to \mathbb{R}$ be a smooth function. We define the* gradient*, denoted by $\nabla f\,(p)$, and the* Hessian*, denoted by $H_f(p)$ of f at p using a chart $(U, \phi = x^1, x^2, \dots x^n)$ about p as follows*

$$\nabla f\,(p) := \left(\frac{\partial f}{\partial x^1}, \frac{\partial f}{\partial x^2}, \dots, \frac{\partial f}{\partial x^n}\right)$$
$$H_f(p) := \left[\frac{\partial^2 f}{\partial x^i\, \partial x^j}\right]_{n\times n}$$

Note that $H_f(p)$ is a symmetric matrix. It is clear from definition that both $\nabla f\,(p)$ and $H_f(p)$ depend on the choice of chart (U, ϕ) about p. Next, we define the notion of a *critical point* and *non-degeneracy of a critical point.*

Definition 1.3.2. *Let M be a smooth n-manifold and $f : M \to \mathbb{R}$ be a smooth function. Let (U, ϕ) be a chart around $p \in M$. The point p is called a* critical point *if $\nabla f\,(p) = (0, 0, \dots, 0)$.*

A priori, being a critical point depends on the choice of the chart used to define $\nabla f\,(p)$ but it can be shown that it does not; hence making the concept well-defined. Also, let C_M denote the collection of all critical points of f on M.

Definition 1.3.3. *Let M be a smooth n-manifold and $f : M \to \mathbb{R}$ be a smooth function. Let (U, ϕ) be a chart around a critical point $p \in M$. The critical point p is called* non-degenerate *if the matrix $H_f(p)$ is invertible and is called* degenerate *otherwise.*

Again, a priori, being a non-degenerate depends on the choice of the chart used to define $H_f(p)$ but it can be shown that it does not; hence making the concept well-defined.

Recall that $H_f(p)$ is a symmetric matrix and is therefore diagonalizable. Let p be a critical point of $f : M \to \mathbb{R}$. Then $H_f(p)$ is invertible and hence has non-zero eigenvalues. Now, we are in a position to define the *index* of a critical point.

Definition 1.3.4. *Let M be a smooth n-manifold and $f : M \to \mathbb{R}$ be a smooth function. Let $p \in M$ be a non-degenerate critical point of f. The number of negative eigenvalues of $H_f(p)$ is defined to be the* index *of p.*

By Sylvester's law of inertia, one can see that the index of a critical point does not depend on the chart used to compute $H_f(p)$ and is hence well-defined. It follows that index of a non-degenerate critical point of a real-valued function defined on a n-dimensional smooth manifold can be any integer in $\{0, 1, 2, \ldots, n\}$. Next, we define *Morse function* and give two important results in Morse theory fundamental to the subject but we do not need them for our study of granular materials.

Definition 1.3.5 (Morse function)**.** *A real valued, smooth function f from a smooth manifold M is called a Morse function if its critical points are non-degenerate.*

Lemma 1.3.1 (Morse lemma)**.** *Let p be a non-degenerate critical point of a real valued smooth function f from a smooth manifold M. Let γ be the index of p. There exists a chart $(x_1, x_2, \ldots, x_n)$ in a neighborhood U of M around p such that for all $q \in U$, we have*

$$f(q) = f(p) - x_1^2 - x_2^2 - \cdots - x_\gamma^2 + x_{\gamma+1}^2 + \cdots + x_n^2$$

Lemma 1.3.2. *Morse functions are dense in the set of all smooth functions.*

It follows from the above lemma that any smooth function can be perturbed to a Morse function. Further, this perturbation can be made as small as necessary. Therefore, in practice, it is okay to assume that the smooth function you are working with is Morse.

1.3.4 Streamlines created by Morse functions

We start by looking at the flow on a smooth manifold M due to a smooth vector field on it. The big picture of have in mind is to think how particles kept at different points on the manifold would move under the influence of of a vector field when it provides it velocity.

Definition 1.3.6. *Let $p \in M$. Let c_p denote the streamline of a particle passing through p under the influence of V. If c_p is parametrized as $c_p : A \subseteq \mathbb{R} \to M$, then it follows the following equation:*

$$\frac{\mathrm{d}c_p}{\mathrm{d}t}(t) = V(t).$$

Streamlines are also called integral lines.

Note that two different streamlines do not intersect. If they would, then at the point of intersection the vector field V will not be uniquely determined.

In the context of Morse theory, the vector field considered is the gradient-like vector field created from a Morse function as described in Section 2.3 in [17]. This rest of this section is adapted from Section 3.1 in [23] and Section 2 in [8].

In the case where V is the gradient-like vector field created from a Morse function (look at [17] for details) and c_p is a streamline passing through p. Then we have the following.

1. If c_p is a maximal integral line, then we can parametrize it as $c_p : \mathbb{R} \to M$.
2. Each integral line is open at the end. $\lim_{t\to\infty} c_p(t)$ is called the *destination* of c_p and $\lim_{t\to-\infty} c_p(t)$ is called the *origin* of c_p.
3. Both $\lim_{t\to\infty} c_p(t)$ and $\lim_{t\to-\infty} c_p(t)$ are critical points.
4. Streamlines cover all regular points, i. e., each regular point on the manifold lies on a streamline.

Note that a streamline never reaches the origin or the destination although it approaches them in the limit. This is because near critical points, the gradient-like vector fields diminish till they vanish on the critical points.

Based on the above properties, we can partition the manifold M into subsets based on where these points would flow under a gradient-like vector field created by a Morse function.

Definition 1.3.7. *Consider a gradient-like vector field created by a Morse function $f : M \to \mathbb{R}$. Let p be a critical point. Let c denote a streamline in M.*

1. *The collection of all (images of) streamlines c on the manifold M such that c has destination p along with p is called the* descending manifold *of p, denoted by* Des_p.
2. *The collection of all (images of) streamlines c on the manifold M such that c has origin p along with p is called the* ascending manifold *of p, denoted by* Asc_p.

One can think of Des_p as the collection of points on M that can reach p through a streamline and Asc_p as the collection of points on M that p can reach through a streamline.

It turns out that for a Morse function having a critical point p of degree k, Des_p is a manifold of dimension k and Asc_p is a manifold of dimension $n-k$ where n is the dimension of the manifold.

Also, note that the descending manifolds of $-f$ are the ascending manifolds of f and vice versa.

We give examples in 1D below.

Example 3. *Examples of ascending and descending manifold in 1D are given below where the vector field is the gradient of the scalar function plotted. In general, ascending manifolds of minimum are the valleys corresponding to the minimum and the descending manifold of a maximum correspond to the mountain corresponding to the maximum.*

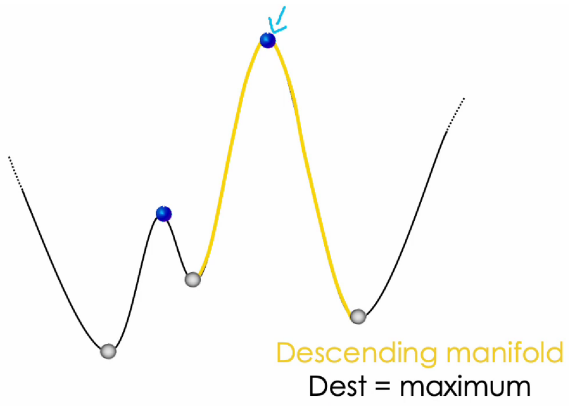

Figure 1.5: Descending manifold of a maximum from [31].

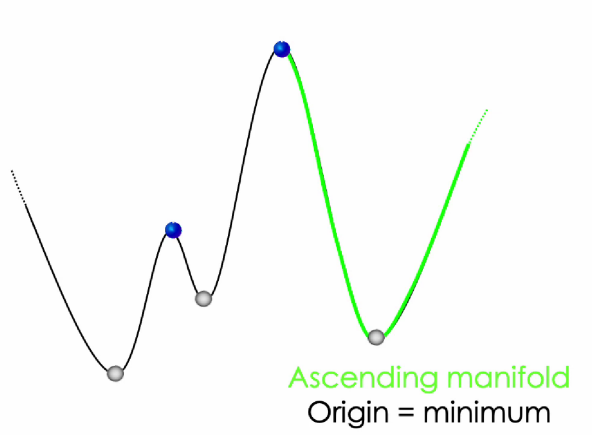

Figure 1.6: Ascending manifold of a minimum from [31].

Since the streamlines are disjoint, different descending manifolds are disjoint and similarly different ascending manifolds are disjoint. Since streamlines cover all the regular points of the manifold, we have that $\{\text{Des}_p \mid p \in C_M\}$ and $\{\text{Asc}_p \mid p \in C_M\}$ form partitions of M. Further, they have a cell structure. The descending manifold of a index k critical point is an open set homeomorphic to $\mathbb{R}^k$. Its boundary is a union of descending manifolds of index $(k-1)$ critical points which form the $(k-1)$-dimensional faces of the k dimensional descending manifold. $\{\text{Des}_p \mid p \in C_M\}$ with its cell structure called the *Morse complex*.

Since the descending manifolds of $-f$ are the ascending manifolds of f and vice versa, we have that the collection of ascending manifolds forms a dual cell structure. $\dim(\text{Asc}_p) = n - \dim(\text{Des}_p)$, Des_q is a face of Des_p if and only if Asc_p is a face of Asc_q. This is akin to the dual block complex defined for a simplicial complex in Section 5.2.

Some illustrations are below. Blue spheres are maxima, blue-grey spheres are 1-saddles and grey spheres are minimas.

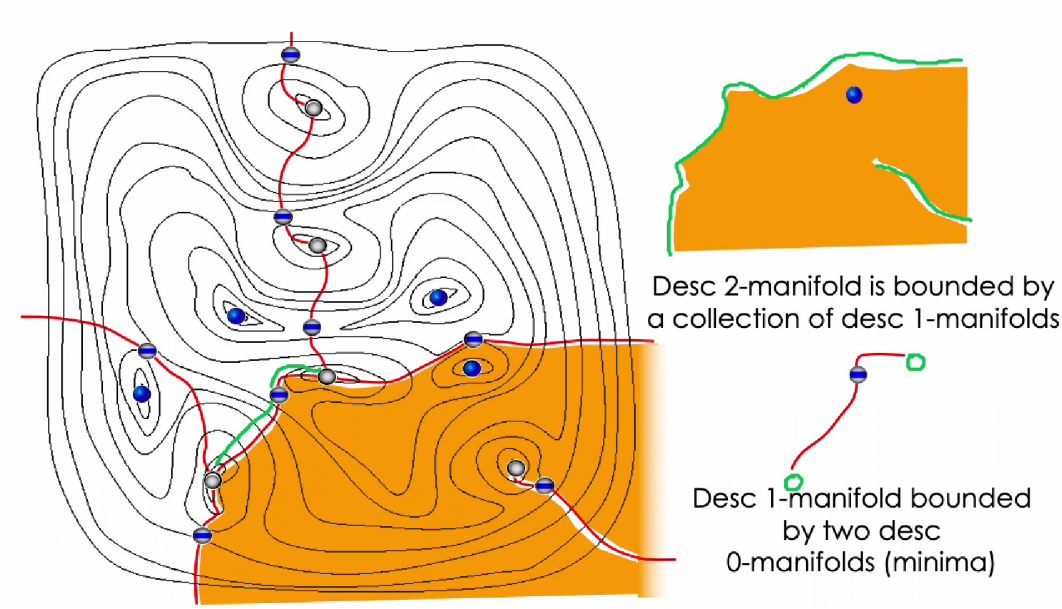

Figure 1.7: Morse complex of 2D terrain from [31]. It has been emphasized that descending 2-manifold of a maximum is bounded by descending 1-manifold of 1-saddles. Descending 1-manifolds of 1-saddles is bounded by descending 0-manifolds of minima.

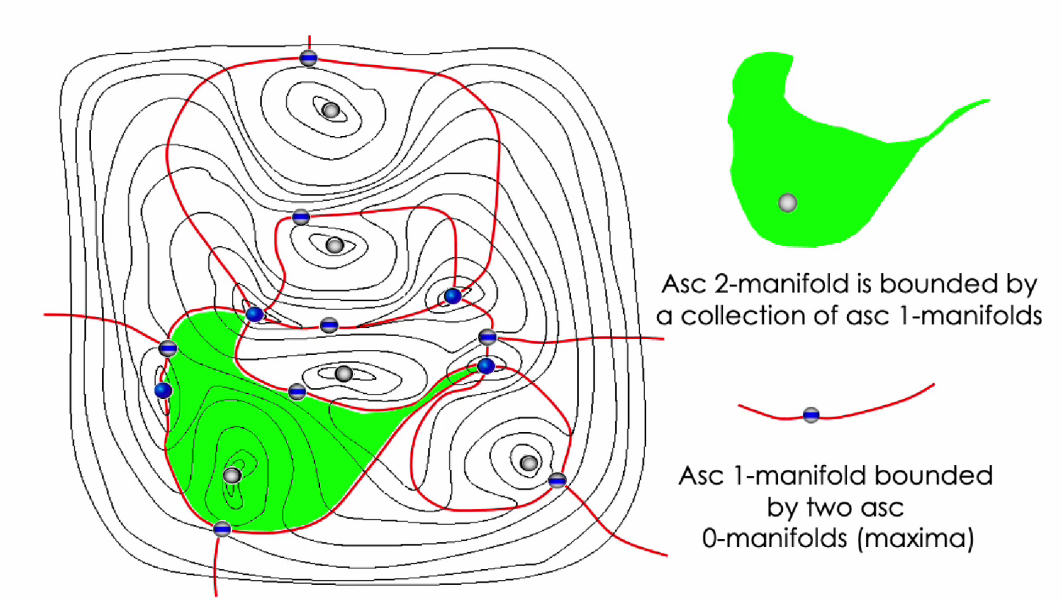

Figure 1.8: Ascending manifolds in 2D terrain from [31]. It has been emphasized that ascending 2-manifold of a minimum is bounded by ascending 1-manifolds of 1-saddles. Ascending 1-manifold of a 1-saddle is bounded by descending 0-manifolds of minima.

The following example's purpose is to highlight the dual cell structure of the Ascending manifolds as described previously in this section.

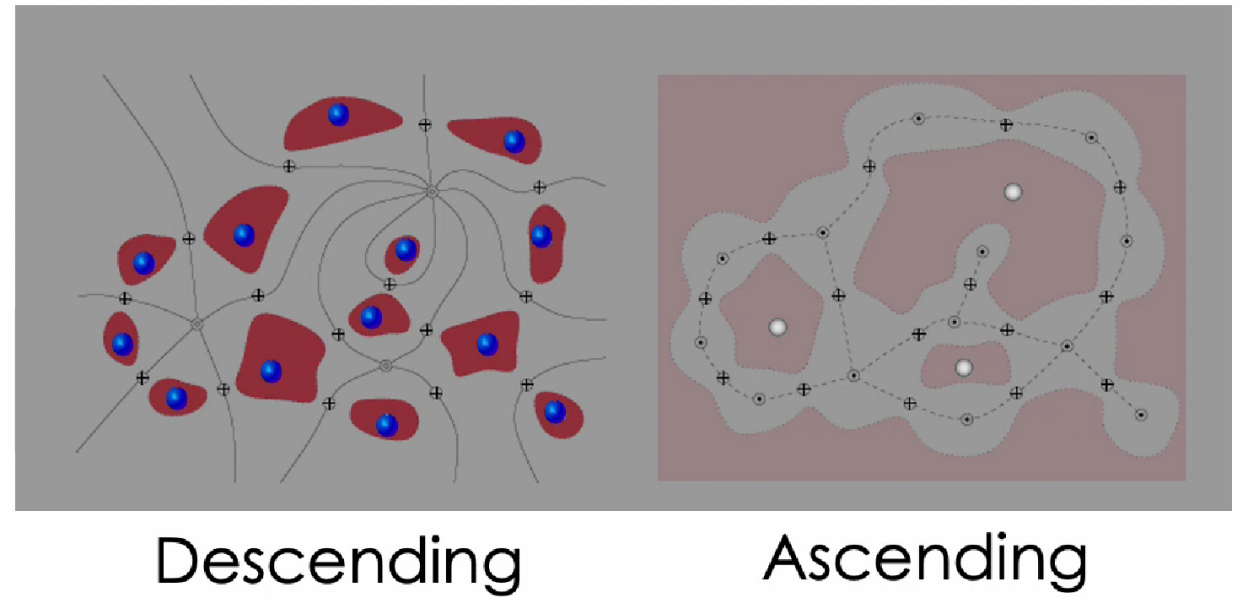

Figure 1.9: Ascending manifolds (right) and (truncated) descending manifolds of a terrain from [31].

1.3.5 The Morse-Smale complex

In the previous section, one considered the Morse complex that partitioned the domain M. For each pair of critical points x, y, $\mathrm{Des}_x \cap \mathrm{Asc}_y$ is the collection of points that lie on streamlines that start from y and end on x. These streamlines have a common origin y and a common destination x. The collection $\{\mathrm{Des}_x \cap \mathrm{Asc}_y \mid x, y \in C_M\}$ is also a partition of M.

We also require the ascending and descending manifolds of a critical point to intersect transversally, i. e., at the point of intersection, the tangent vectors are not parallel[1]. Once this condition is met, the collection $\{\mathrm{Des}_x \cap \mathrm{Asc}_y \mid x, y \in C_M\}$ is called the *Morse Smale complex*, denoted by MS_M. Each element in MS_M is called a *Morse Smale cell*. Without the Morse-Smale condition, the Morse Smale complex would not be a cell complex.

In the example given in the Figure 1.9, the Morse Smale complex is the following.

[1]If there are non-transversal intersections, one can perturb the Morse function to avoid them.

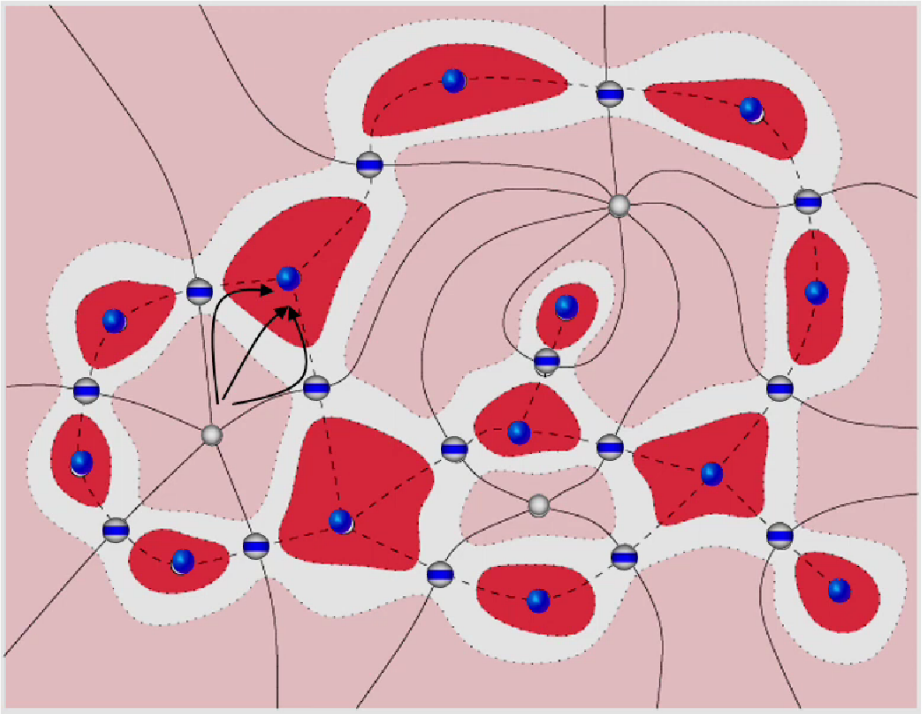

Figure 1.10: Morse-Smale complex of a 2D terrain from [31].

The Morse-Smale complex also has a nice cell structure hiighlighed in the following properties.

1. The MS complex consists of 0-cells, 1-cells, 2-cells, etc.

2. A 3-cell is bounded by 4 2-cells, a 2-cell is bounded by 4 1-cells, a 1-cell is bounded by 2 0-cells.

Since each cell of a MS complex does not contain critical points, each cell is monotonic. We can ignore the monotonic nature of cells and represent a MS complex as a graph. This only keeps the combinatorial structure of the MS complex. The following figure shows the combinatorial representation of the MS complex shown in Figure 1.10.

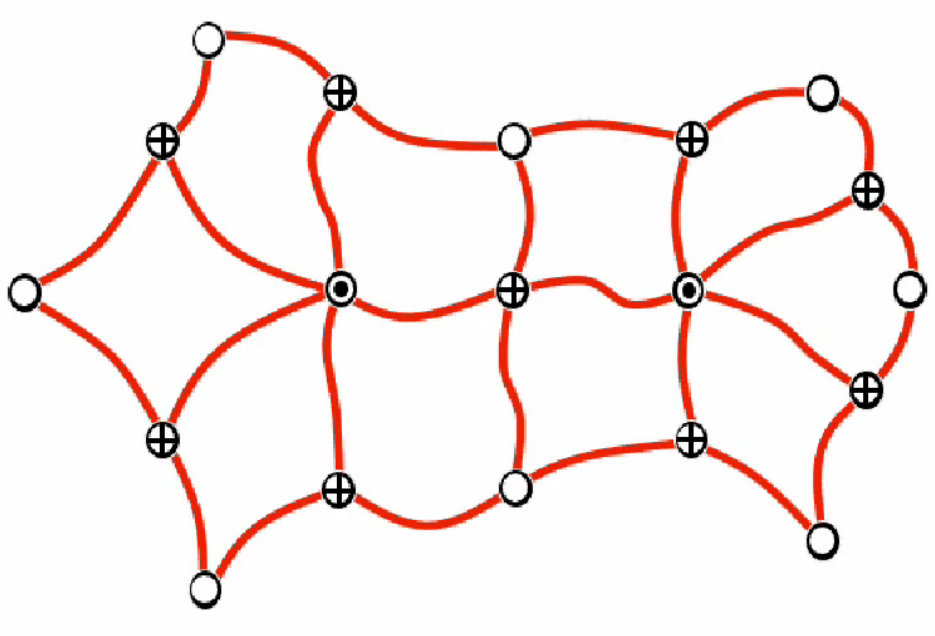

Figure 1.11: Combinatorial representation of MS complex of the 2D terrain in Figure **??**. Image taken from [31].

In general, the combinatorial structure of a 2D MS complex has the following properties.

1. Nodes correspond to critical points.
2. Saddles have 2 arcs incident on them.
3. All regions are quads.

The combinatorial structure of MS complex in 3D is as follows.

1. Nodes are critical points.
2. Arcs connect critical points whose index differ by 1.
3. 2D cells are quads.
4. Crystals (3D cells) always have 1 min, 1 max and quads on their boundary.
5. Arcs connecting saddles have a 'ring' of quads around them.

1.4 Voronoi tesselation, Delaunay complex and Medial axis

In this section, we will discuss about Voronoi tesselation, its 'dual' notion the Delaunay complex and their connections with the medial axis. The main references for this section are [18] and Section 2 in [19].

The essential idea of the medial axis is that it consists of points that, roughly speaking, lie in the middle of a space, i. e., points in the space at equal distance from points on the medial axis. The Voronoi tesselation of a finite subset of points in a space is a partition of the space into regions that are closest to points. The Voronoi tesselation is related to the medial axis because if finds regions closest a finite subset of points then the points common to regions corresponding to a few of the points are equidistant from those points. The Delaunay complex naturally captures this by creating a simplex corresponding to intersections between the Voronoi regions. Now, we begin by defining everything rigorously.

1.4.1 Voronoi Regions

Definition 1.4.1. *Let $p_1, p_2, \ldots, p_m$ be unique points in $\mathbb{R}^n$.* Voronoi region *of p_k, $V(p_k)$ is the set of all points in $\mathbb{R}^n$ closer to p_k than p_l for $l \neq k$, i. e.,*

$$V(p_k) = \{x \in \mathbb{R}^n \mid |x - p_k| \leq |x - p_l| \text{ for } l \neq k\}$$

Below is a figure from [33] showing the Voronoi regions for 20 points in a plane.

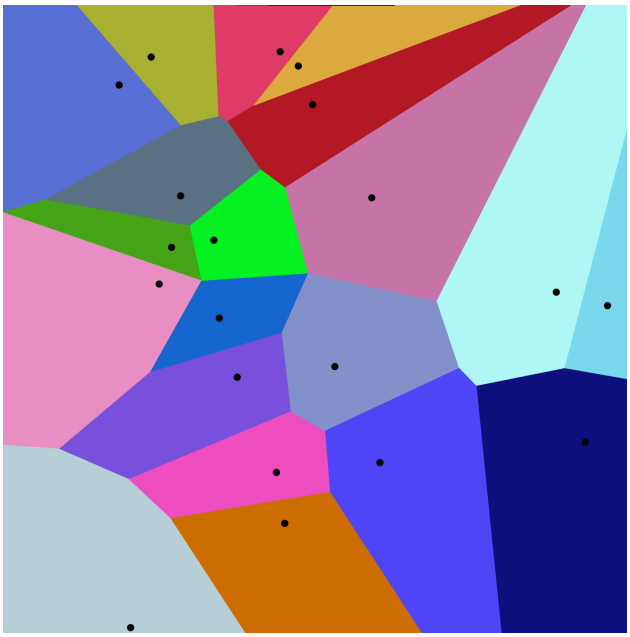

Figure 1.12: Voronoi regions for 20 points in the plane.

We denote the collection of all Voronoi regions of $\{p_1, p_2, \ldots, p_m\}$ by $\mathrm{Vor}(p_1, p_2, \ldots, p_m)$. Below are some properties of Voronoi regions.

1. Each Voronoi region is an intersection of finitely many closed half planes and is therefore a closed convex polyhedron.

2. $\mathrm{Vor}(p_1, p_2, \ldots, p_m)$ covers $\mathbb{R}^n$

3. Interiors of Voronoi regions are pair-wise disjoint.

Intersections of more than one Voronoi regions is called a *Voronoi cell*.

Classically, one defines Voronoi cells for points in $\mathbb{R}^n$. One might as well define them for finite number of compact subsets using a notion of distance from compact subsets for example distance of a point b from a subset A can be defined by $\mathrm{Inf}\,(|b-a| \mid a \in A)$. Such notion has been discussed in [18] where they give an algorithm to find the medial axis of a system of spheres of possibly different radii. Next, we discuss about the Delaunay complex.

1.4.2 Delaunay Complex

Definition 1.4.2. *Let $p_1, p_2, \ldots, p_m$ be unique points in $\mathbb{R}^n$. The* Delaunay complex *of these points is the simplicial complex with vertex set $\{p_1, p_2, \ldots, p_m\}$ whose simplices are defined as follows.*

$$[p_{i_1}, p_{i_2}, \ldots, p_{i_f}] \text{ is a face } \iff \exists x \in \mathbb{R}^n \text{ equidistant from the points } p_{i_1}, p_{i_2}, \ldots, p_{i_f}$$

It follows from the above definition that the simplices in the Delaunay complex are in one-to-one correspondence to the Voronoi cells. Alternatively, the Delaunay complex is the nerve of the Voronoi regions:

$$\{\sigma \subset \text{Vor}(p_1, p_2, \ldots, p_m) \mid \bigcap_{a \in \sigma} a \neq \emptyset\}$$

There is also an alternate characterization of Delaunay complex based on empty spheres passing through a subset of points $\{p_1, p_2, \ldots, p_m\}$ but we do not mention it here. One can check Section 2 in [19]. Such characterization exists because spheres are locus of points equidistant from the center of the sphere. If there is a empty sphere (empty meaning there are no points from $\{p_1, p_2, \ldots, p_m\}$ inside it) passing through a subset of points in $\{p_1, p_2, \ldots, p_m\}$ then its center lies on a Voronoi cell.

Lastly, we discuss the 'duality' between Voronoi regions and Delaunay complex. This is duality is there because of the following correspondence we discussed before – the simplices in the Delaunay complex are in one-to-one correspondence to the Voronoi cells. The duality we speak of here tells us that the Voronoi regions and the Delaunay complex are two sides of the same coin. Both of them carry the same information in two different ways – Voronoi cells are collections of points in $\mathbb{R}^n$ equidistant from some points in $\{p_1, p_2, \ldots, p_m\}$ and those points form a simplex in the Delaunay complex.

The reason I got interested in Voronoi-Delaunay stuff was to see if I could model a subspace by one of Voronoi or Delaunay and its complement by the other. I do not think that is possible.

Lastly, we discuss the Medial axis which is somewhat related to Voronoi and Delaunay ideas.

1.4.3 Medial axis

The medial axis of a space, informally speaking, is a subset of that space that is geometrically similar to that space. It is sometimes also referred to as a topological skeleton of the space. For example, take a look at the figure below taken from https://3d.bk.tudelft.nl/projects/3dsm/.

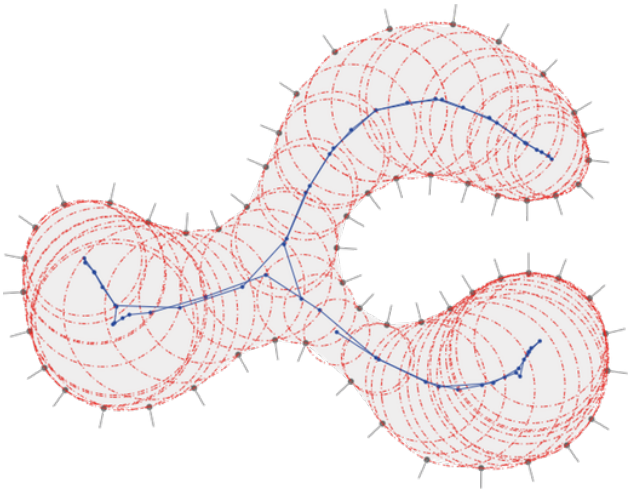

Figure 1.13: Medial axis of a finite collection of points in the plane

Formally, the medial axis is an attempt to approximate a subset of space by fitting big balls in that space. As described in [4], the *medial axis transform* of a subset $A \subset \mathbb{R}^n$, denoted by $MAT(A)$, is the topological closure of the set of points (x, r) such that the ball centered at $x \in A$ with radius r is locally maximal. The collection of all points x such that $(x, r) \in MAT(A)$ for some r is called the medial axis of A.

Equivalently, the medial axis is the set of points having at least one closest point on the object's topological boundary. This definition is equivalent to the previous definition of finding maximal inscribed balls because once you have a closest point that on the boundary it specifies a unique ball that is maximal. If there are multiple closest points on the boundary, since they are at the same distance away from the center of the ball, they specify the same ball.

As we pointed to earlier, there is a connection between Voronoi cells and the Medial axis. If you find the medial axis of a finite collection of points in $\mathbb{R}^n$, then this contains the union of Voronoi cells of the collection of points.

1.5 Persistence

Persistence is the idea that features would persist over noise. Persistent homology, built on this idea, is a framework to capture persistent homological features. In order to talk about persistence of something, we need to first talk about how the situation is changing. In a topological setting, we consider a finite sequence of topological spaces, $(X_1, X_2, \ldots, X_n)$, and continuous maps connecting them $f_i : X_i \to X_{i+1}$ as follows:

$$X_1 \xrightarrow{f_1} X_2 \xrightarrow{f_2} \cdots \xrightarrow{f_{n-1}} X_n, \tag{1.1}$$

where we can track how topological features change though the maps f_is and which features persist. Usually, the spaces X_i form a *filtration*, i. e., $X_i \subset X_{i+1}$ for all i and the maps f_i are inclusions of X_i into X_{i+1}. The primary reference for this section is [7].

1.5.1 Persistent homology

For a given filtration $X_1 \subseteq X_2 \subseteq \cdots \subseteq X_n$ to look persistent homological features, we look at the induced sequence of homology groups and homomorphisms between them for each dimension k

$$\mathrm{H_k}(X_1) \xrightarrow{f_k^{12}} \mathrm{H_k}(X_2) \xrightarrow{f_k^{23}} \cdots \xrightarrow{f_k^{(n-1)n}} \mathrm{H_k}(X_n) \tag{1.2}$$

where $f^{ij} : X_i \to X_j$ are inclusion of X_i into X_j and $f_k^{ij} : \mathrm{H_k}(X_i) \to \mathrm{H_k}(X_j)$ are the induced homomorphisms on the homology groups.

If one follows a homology class in any homology group, say, $H_k(X_i)$, then either f_{i*} maps it to 0 or it maps it to a non-zero homology class in $H_k(X_{i+1})$. One can start with cycles in $H_k(X_1)$ and keep track of them as one moves in the sequence of maps (1.2). This is the idea behind a *persistent module*. Naturally, we want to track when homological features are *born* and when they *die*. We give precise definitions below.

Definition 1.5.1. *The* kth persistent homology groups*, denoted by,* $H_k^{i,j}$ *are defined to be* $\mathrm{im}(f_k^{i,j})$ *and* $H_k^{i,i}$ *are defined to be* $\mathrm{H_k}(X_i)$ *The* kth persistent Betti numbers *are ranks of these groups, i. e.,* $\beta_k^{ij} = \mathrm{rank}(H_k^{i,j})$.

The kth persistent homology group captures what homological features are old, i. e., they

were present before. More concretely, $H_k^{i,j}$ consist of features in $\mathrm{H_k}(X_i)$ that are still alive in $\mathrm{H_k}(X_j)$.

Definition 1.5.2. *A feature $\gamma \in \mathrm{H_k}(X_i)$ is said to be* born *at X_i if $\gamma \notin H_k^{i-1,i}$. A feature γ born at X_i is said to* die entering *X_j if it merges with an older class as we go from X_{j-1} to X_j, i. e., $f_k^{i,j-1}(\gamma) \notin H_p^{i-1,j-1}$ but $f_k^{i,j}(\gamma) \in H_k^{i-1,k}$.*

Persistence of a feature is captured by the amount of time a feature lives.

Definition 1.5.3. *If γ in born at X_i and dies at X_j, then the* index persistence *of γ is the difference in the index, i. e., $j - i$. If X_is are level sets, i. e., $X_i = f^{-1}[a_i, \infty)$, then the persistence of γ is defined to be the difference $a_j - a_i$.*

If γ is born but it never dies, then we define both its index persistence and persistence to be ∞.

Note that there can be many features that are born at X_i and die entering X_j. Let $\mu_k^{i,j}$ be the number of k-dimensional classes that are born at X_i and die entering X_j. We have $\mu_k^{i,j} = (\beta_k^{i,j-1} - \beta_k^{i,j}) - (\beta_k^{i-1,j-1} - \beta_k^{i-1,j})$. The first difference is the number of features born at or before X_i and die entering X_j and the second difference is the number of features born at or before X_{i-1} and die entering X_j.

1.5.2 Persistence diagrams

A persistence diagram is a scatter plot of the birth death pairs for each feature. There are two important points to discuss. First, some death values can be ∞ and hence, we need to plot the points on the extended real plane. Second, there can be multiple features for the same birth death pair – as discussed in the previous section, there are $\mu_k^{i,j}$ number of them. Hence, the scatter plot has multiset of points. The nice thing about the persistence diagram is that the distance of a point from the *birth* = *death* line gives us the persistence of a feature. This distance also equals the vertical distance of a point from the *birth* = *death* line.

The important property of persistence diagram is that they are immune to noise in the sense that they are stable with respect to small changes in the function that defines the level set filtration for which persistence diagrams have been computed.

1.5.3 Persistence curve

If one computes the persistence diagram for a filtration, there will be points with a range of persistence. One of our motivations for discussing persistence was to separate features that do not occur from noise. In order to do that, one needs to specify a *cutoff* persistence value – all features with persistence less than the cutoff are considered noise. Usually, there is no canonical way to do this. In practice, this is done via hit and trial. But there is a better way of doing this which uses the persistence curve.

The *persistence curve* for a filtration is a plot of number of features with persistence greater than x against X. To choose the cutoff persistence, one uses the x value that corresponds to a knee in the persistence curve. This is a good choice because a knee in the curve (a point where derivative of the curve changes abruptly) which separates high persistence features from relatively low persistence features. The excellent thing about the knee in the persistence curve is that it is completely intrinsic to the data and hence more objective than any user input cutoff.

This idea is used in [23] to find a cutoff for simplifying the Morse Smale complex by removing noisy features from it leading to a accurate particle segmentation.

1.6 Alexander duality

Let X be a topological space. Given a subset A of X we can find its homology and cohomology groups. Informally speaking, since homology of A tells us about the holes in A and if we know them, we should also be able to say something about the holes in the complement $X \setminus A$. Alexander duality is an answer to this question when the topological space X is the n-sphere S^n. We give the following version from [11].

Theorem 1.6.1. *Let A be a non-empty, proper, compact, locally contractible subspace of S^n, then $\widetilde{\mathrm{H}}_{\mathrm{k}}(S^n \setminus A) \cong \widetilde{\mathrm{H}}^{\mathrm{n-k-1}}(A)$ for all $k \in \{0, 1, 2, \ldots, n-1\}$.*

This result apriori seems unnatural. Why would the reduced cohomolgy of A relate to the reduced homology of the complement $S^3 \setminus A$? To get some feel for it, consider the following example for $k = 1$. Let A be a graph embedded tamely in $X = S^3$. Let α be a (non-trivial)

1-cycle in the complement $S^3 \setminus A$ representing an element of $\mathrm{H}_1(S^3 \setminus A)$. Since α is not a boundary, it needs to pass through some cycles (that are not boundaries) in A, i. e., it links with a few cycles in A. Hence, we can define a function on $f_\alpha : \mathrm{H}_1(A) \to \mathbb{Z}$ which maps each cycle in $\mathrm{H}_1(A)$ to its linking number with α. Also, if we choose a set of basis cycles $\beta_1, \beta_2, \ldots, \beta_l$ in $\mathrm{H}_1(A)$ each along with an integer n_j functioning as a linking number allowing for zero linking number zero, then we can find a cycle $\alpha^{n_1,n_2,\ldots,n_l}_{\beta_1,\beta_2,\ldots,\beta_l}$ in $\mathrm{H}_1(S^3 \setminus A)$ that links with β_j with linking number n_j. Hence, it seems that the map f_α is an isomorphism between $\mathrm{H}_1(S^3 \setminus A)$ and $\mathrm{Hom}\left(\mathrm{H}_1(A), \mathbb{Z}\right)$. Since A has no torsion, then $\mathrm{Hom}\left(\mathrm{H}_1(A), \mathbb{Z}\right) \cong \mathrm{H}^1(A)$ and we get that $\mathrm{H}_1(S^n \setminus A) \cong \mathrm{H}^1(A)$. Alexander duality is a generalization of this that works for all dimensions and even in the cases where there is torsion.

We also give a reformulation of this result for $\mathbb{R}^n$ since we would be working with granular materials in $\mathbb{R}^3$. We do this using one-point compactification. We start by recalling it from [21], refer to Theorem 29.1.

Proposition 1.6.2 (One-point compactification)**.** *Let X be a locally compact Hausdorff topological space. Then there exists a compact Hausdorff space Y such that $Y \setminus X$ is a point. Let $c : X \to Y$ be the inclusion of X into Y. Then the map c is an continuous, open map.*

Let $Y \setminus X = \{\infty\}$. The open sets of Y are precisely

1. open subsets of X seen as open subsets of Y through c,
2. the sets $Q \cup \{\infty\}$ where Q is complement of a compact subset of X.

Note that if $A \subset X$ is locally contractible. then $c(A) \subset Y$ is also locally contractible since open maps preserve local contractibility.

The most well-known example of one-point compactification is that the one-point compactification of $\mathbb{R}^n$ is homeomorphic to S^n. Let us again denote the extra point in S^n by $\{\infty\}$. Now, we are ready to give a version of Alexander duality for $\mathbb{R}^n$.

Theorem 1.6.3 (Alexander duality for $\mathbb{R}^n$)**.** *Let A be a non-empty, proper, compact, locally contractible subspace of $\mathbb{R}^n$. Then*

$$\mathrm{H}_0(\mathbb{R}^n \setminus A) \cong \mathrm{H}^{\mathrm{n-1}}(A) \oplus \mathbb{Z},$$
$$\mathrm{H}_{\mathrm{k}}(\mathbb{R}^n \setminus A) \cong \mathrm{H}^{\mathrm{n-k-1}}(A), \ \textit{for } k \in \{1, 2, \ldots, n-1\}.$$

Proof. Let $B = A \cup \{\infty\}$. Note that $\mathbb{R}^n \setminus A = S^n \setminus B$. Further, since A is non-empty, proper, compact, locally contractible subspace of $\mathbb{R}^n$, B is non-empty, proper, compact, locally contractible subspace of S^n. Therefore, we can apply Alexander duality 1.6.1 to get

$$\widetilde{\mathrm{H}}_{\mathrm{k}}(S^n \setminus B) = \widetilde{\mathrm{H}}^{\mathrm{n-k-1}}(B)$$

for all $k \in \{0, 1, 2, \ldots, n-1\}$. Since $\mathbb{R}^n \setminus A = S^n \setminus B$, and $B = A \cup \{\infty\}$, we get

$$\widetilde{\mathrm{H}}_{\mathrm{k}}(\mathbb{R}^n \setminus A) = \widetilde{\mathrm{H}}^{\mathrm{n-k-1}}(A \cup \{\infty\}) .$$

If $n - k - 1 \neq 0$, i. e., $k \leq n - 2$, reduced cohomology is just the cohomology, and we get

$$\widetilde{\mathrm{H}}_{\mathrm{k}}(\mathbb{R}^n \setminus A) \cong \mathrm{H}^{\mathrm{n-k-1}}(A \cup \{\infty\}) .$$

Now, using the fact the cohomology of disjoint spaces add, we have,

$$\widetilde{\mathrm{H}}_{\mathrm{k}}(\mathbb{R}^n \setminus A) \cong \mathrm{H}^{\mathrm{n-k-1}}(A \cup \{\infty\}) \cong \mathrm{H}^{\mathrm{n-k-1}}(A) \oplus \mathrm{H}^{\mathrm{n-k-1}}(\{\infty\}) .$$

Since $\{\infty\}$ is a point, its cohomology groups vanish, and we have for $\{0, 1, 2, \ldots, n-2\}$,

$$\widetilde{\mathrm{H}}_{\mathrm{k}}(\mathbb{R}^n \setminus A) \cong \mathrm{H}^{\mathrm{n-k-1}}(A) .$$

For $k = n - 1$, we have

$$\widetilde{\mathrm{H}}_{\mathrm{n-1}}(\mathbb{R}^n \setminus A) \cong \widetilde{\mathrm{H}}^0(A \cup \{\infty\}) .$$

Using UCT, we have $\widetilde{\mathrm{H}}^0(A \cup \{\infty\}) \cong \mathrm{Hom}\left(\widetilde{\mathrm{H}}_0(A \cup \{\infty\}), \mathbb{Z}\right)$, and since $\{\infty\}$ is a point, $\widetilde{\mathrm{H}}_0(A \cup \{\infty\}) = \mathrm{H}_0(A)$. We finally have

$$\widetilde{\mathrm{H}}_{\mathrm{n-1}}(\mathbb{R}^n \setminus A) \cong \mathrm{Hom}\left(\mathrm{H}_0(A), \mathbb{Z}\right) .$$

Now, again invoking UCT, we have that $\mathrm{Hom}\left(\mathrm{H}_0(A), \mathbb{Z}\right) \cong \mathrm{H}^0(A)$.

The statement in the theorem now follows if once unwraps the definition of reduced homology. □

Remark 1.6.1. *In fact, there is a version of statement of the above theorem with $\mathbb{R}^n$ replaced with the n-ball B^n given that the pair (B^n, A) is triangulate. Refer to Exercise 5, pp. 426 in [20].*

We give explicit relations for $n = 2, 3$ because they are the only ones relevant to us.

$n = 2$

$$\begin{aligned} \mathrm{H}_0\left(\mathbb{R}^2 \setminus A\right) &\cong \mathrm{H}^1(A) \oplus \mathbb{Z} \\ \mathrm{H}_1\left(\mathbb{R}^2 \setminus A\right) &\cong \mathrm{H}^0(A) \end{aligned}$$

$n = 3$

$$\begin{aligned} \mathrm{H}_0\left(\mathbb{R}^3 \setminus A\right) &\cong \mathrm{H}^2(A) \oplus \mathbb{Z} \\ \mathrm{H}_1\left(\mathbb{R}^3 \setminus A\right) &\cong \mathrm{H}^1(A) \\ \mathrm{H}_2\left(\mathbb{R}^3 \setminus A\right) &\cong \mathrm{H}^0(A) \end{aligned}$$

The following lemma gives relations between Betti numbers of $A \subseteq \mathbb{R}^n$ and its complement $\mathbb{R}^n \setminus A$ which follow from Theorem 1.6.3.

Lemma 1.6.4. *Let A be a non-empty, proper, compact, locally contractible subspace of $\mathbb{R}^n$. Then*

$$\begin{aligned} \beta_0\left(\mathbb{R}^n \setminus A\right) &= \beta_{n-1}\left(A\right) + 1 \\ \beta_k\left(\mathbb{R}^n \setminus A\right) &= \beta_{n-k-1}\left(A\right) \end{aligned}$$

Proof. Theorem 1.6.3 gives us

$$\begin{aligned} &\mathrm{H}_0(\mathbb{R}^n \setminus A) \cong \mathrm{H}^{\mathrm{n}-1}(A) \oplus \mathbb{Z}, \\ &\mathrm{H}_{\mathrm{k}}(\mathbb{R}^n \setminus A) \cong \mathrm{H}^{\mathrm{n}-\mathrm{k}-1}(A)\,, \text{ for } k \in \{1, 2, \ldots, n-1\}. \end{aligned}$$

Recall that the cohomology groups and homology groups have same rank. The content of the theorem follows immediately. □

Again, we give explicit relations for $n = 2, 3$ because they are the only ones relevant to us.

$n = 2$

$$\begin{aligned}\beta_0\left(\mathbb{R}^2 \setminus A\right) &= \beta_1(A) + 1\\ \beta_1\left(\mathbb{R}^2 \setminus A\right) &= \beta_0(A)\end{aligned}$$

$n = 3$

$$\begin{aligned}\beta_0\left(\mathbb{R}^3 \setminus A\right) &= \beta_2(A) + 1\\ \beta_1\left(\mathbb{R}^3 \setminus A\right) &= \beta_1(A)\\ \beta_2\left(\mathbb{R}^3 \setminus A\right) &= \beta_0(A)\end{aligned}$$

As an example, let us discuss (planar) graphs in $\mathbb{R}^2$.

Example 4. *Let G be a finite planar graph with v vertices, e edges and c connected components. It is well-known that the Betti numbers of G are*

$$\begin{aligned}\beta_0(G) &= c,\\ \beta_1(G) &= e - v + c.\end{aligned}$$

Let us find the Betti numbers of complement of G in $\mathbb{R}^2$. We use the following figure to illustrate the idea. As one can see, the complement $\mathbb{R}^2 \setminus G$ has $f + 1$ connected components where f is the number of (bounded) faces of G. Each face in G gives one component and there is one unbounded component totaling $f + 1$. Since f equals $\beta_1(G)$, we get that $\beta_0(\mathbb{R}^2 \setminus G) = \beta_1(G) + 1$. There are c independent cycles in the unbounded component of $\mathbb{R}^2 \setminus G$, one corresponding to each connected component of G. The f bounded connected components of $\mathbb{R}^2 \setminus G$ do not contribute to $\beta_1(\mathbb{R}^2 \setminus G)$. Therefore, $\beta_1(\mathbb{R}^2 \setminus G) = c$. We get that $\beta_1(\mathbb{R}^2 \setminus G) = \beta_0(G)$. The results are in accordance to the formulas (1.6).

We end this section with the following observation.

Lemma 1.6.5. *Let A, B be homotopy equivalent subspaces of $\mathbb{R}^n$. Then the homology groups of their complements are isomorphic, i. e., $\mathrm{H_k}(\mathbb{R}^n \setminus A) \cong \mathrm{H_k}(\mathbb{R}^n \setminus B)$ for all $k \in \{0, 1, 2, \ldots, n-1\}$.*

Proof. This is a straightforward consequence of Theorem 1.6.3. If A and B are homotopy equivalent, then they have same cohomolgy groups. Since Theorem 1.6.3 relates the homology groups of a subspace of $\mathbb{R}^n$ with its cohomology groups, we get that $\mathrm{H_k}(\mathbb{R}^n \setminus A) \cong \mathrm{H_k}(\mathbb{R}^n \setminus B)$ for all $k \in \{0, 1, 2, \ldots, n-1\}$. □

1.7 Percolation threshold

The term 'Percolation' originally was used for the motion movement of fluids through porous materials. For the purpose of this thesis, we follow the definition of *percolation threshold* given in [26].

Definition 1.7.1. *Given a bounded subset X of $\mathbb{R}^3$. The radius of the largest sphere that can be made to move through X is defined to be the* percolation threshold *of X.*

Remark 1.7.1. *Note that the phrase "move through X" is ambiguous for general $X \subset \mathbb{R}^3$. We would be working with percolation threshold for different phases of granular materials and there the phrase "move through " is clear.*

Such notions are useful when one considers a setup where particles are made to fall under gravity through a bed of larger particles as done in [34]. For such considerations, we also need to give X the notion of side, since particles go through one side of X to the other side.

Let X_a defined as the collections of points in X at least distance a away from the boundary of X. [26] mentions that there is a connection between finding the percolation threshold and considering the path connectivity of level sets X_a – percolation threshold r is largest value of a for which X_a 'spans' the X, i. e., there is a path from one side of X to the other side of X.

1.8 Topics from Image Processing

(Digital) Image processing is the subject that studies various mathematical techniques implemented in order to manipulate digital images. Since we would be working with grayscale images in Section 2.2, we discuss the relevant techniques here. For the discussion here, we will think of grayscale images as functions mapping pixels to values in $[0, 1]$.

1.8.1 Thresholding

Given a grayscale image img : pixels $\to [0, 1]$, and a threshold $t \in [0, 1]$, thresholding re-assigns intensity value 1 to pixels having intensity value greater than t and intensity value

0 to pixels having intensity values less than t thereby creating a binary image. In practice, choosing the threshold t is non-trivial and various techniques have been devised to choose good thresholding values such that the thresholded image is meaningful.

The most famous thresholding method is *Otsu's thresholding* which finds the threshold by minimizing a certain intra-class variance. The problem with this method is that it finds a threshold that is globally optimal without attention to local details.

The *Active Contours Without Edges (ACWE)* method minimizes the intra-class variance both inside and outside the boundary $\text{img}^{-1}(t)$ to find the threshold. This method is superior for incorporating local features of an image. This will be important to us when we segment granular materials – we would use thresholding to find the boundary surface of the granular material. The quality of segmentation depends directly on the quality of such a boundary surface which should be sensitive to the local variation in the geometry of the particles.

1.8.2 Euclidean distance transform

Given a binary image $\text{img} : \text{pixels} \to [0, 1]$, where $A \subset \text{pixels}$ is the boundary of the foreground ($\text{img}^{-1}(1)$) and background ($\text{img}^{-1}(0)$). The Euclidean distance transform of img is an image $EDT(\text{img}) : \text{pixels} \to \mathbb{R}$ that maps each pixel to the (Euclidean) distance from A. The Euclidean distance transform of an image is thus a scalar field on the domain pixels.

1.8.3 Watershed methods

The watershed methods are a class of techniques used to segment grayscale images. As their name indicates, these are inspired from watersheds in geology which separate drainage basins. We will briefly discuss the most common method called *watershed by flooding* from [3].

This method segments different regions of a grayscale image that correspond to unique minima by drawing a boundary around it. Continuing the geological analogy, we know that water flows from different points on a topographic surface to a local minimum of the height function. The collection of all points that lead to flow of water into a minimum is called the *catchment basin* of the minimum. Different catchment basins intersect in *watersheds*, which are boundaries that separate different watersheds. Now, the idea is to reverse this process for

images. The pixels of the image are thought to make the topographic region and the height function is thought of as the grayscale value assigned to each pixel. We let water level rise from the minima and let them fill their catchment basins. As the water level rises, different catchment basins meet in watersheds. This is done rigorously in [3] as follows.

Let img : pixels $\to [0,1]$ be a grayscale image. Define the level sets $X_a = \{x \in \text{pixels} \mid \text{img}(x) \leq a\}$ and $X_a = \{x \in \text{pixels} \mid \text{img}(x) < a\}$.

Remark 1.8.1. *The level sets X_a completely specify the function* img. *This is because* $\text{img}(x) = \text{Inf}\,(a \mid x \in X_a)$.

Next, the authors define the geodesic distance. Let x, y be two points in a $X \subset \mathbb{R}^n$. $d_X(x,y)$ is defined to be the smallest length of the curve that starts at x and stops at y, i. e., $d_X(x,y) = \text{Inf}\,(len(c) \mid c : [0,1] \to X$ continuous with $c(0) = x, c(1) = y)$ and it is defined to be ∞ is no such curve exists. The reason for this choice of distance is because X may be a very non-convex region as in the figure below.

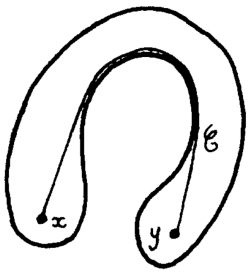

Figure 1.14: Figure 1 from [3] showing the reason to use geodesic distance over other metrics.

The authors then give an alternate characterization of minima. img has a minimum at x of value a if $d_{X_a}(x, Y_a) = \infty$.

Given a point of $x \in X$ and a subset $Y \subset X$, we define the distance of x from Y by $d_X(x,Y) = \text{Inf}\,(d_X(x,y) \mid y \in Y)$.

Let $Y \subset X$ and $P_1, P_2, \ldots P_n$ be pairwise disjoint subsets of Y that cover it. Then the authors define the zone of influence of P_k, denoted by $I_p(Y;X)$, to be the collection of all points of X at finite distance from P_k and closer to P_k than P_l for $l \neq k$. Note that the points of X that do not belong to any zone of influence are points at ∞ distance from Y or

points that are equidistant from at least two P_ks. The collection of later points is called the skeleton by zone of influence of of Y with respect to X and is denoted by $S(Y; X)$ when the partition $P_1, P_2, \ldots P_n$ is clear from context.

Finally, we define catchment basin and watersheds sort of inductively. Let Z be the collection of all points in the watershed, Z_a be the collection of points in watersheds with img value a. We obviously have $Z = \bigcup_a Z_a$. Suppose we know Z_a for all values strictly less than b. Using this information, we will find the watershed Z_b. Note that $Y_b \setminus \bigcup_{a<b} Z_a$ is the collection of all points whose img value is less than b. These points belong to exactly one catchment basin. Then we define $Z_b = S\left(Y_b \setminus \bigcup_{a<b} Z_a; X_b\right)$.

Chapter 2

Introduction to Granular materials and their study

2.1 What are Granular materials?

Granular materials are collections of discrete macroscopic entities called particles. It is obvious that when different particles come together in a container, there are empty spaces around the particles that are created because the particles do not fit into each other perfectly. These empty spaces are called voids or pores.

Granular materials comprise of a very important class of materials and their examples span across diverse domains: geological materials (sand, soil, snow, rocks) to microbiological materials (drug delivery systems, clusters of microbes) to industrial materials (cement, concrete, powders and mixtures) to simple household materials (nuts in a jar, granular sugar) and many more. The study of granular materials benefits all of the domains in which they occur: understanding landslide and avalanche mechanism, designing better drug delivery systems, optimizing mixtures in industrial settings or using brazil nut effect to separate your favorite nut from a mixture! If you loosen up your definition of a particle, one might also call a gathering of humans as a granular material thinking of each human as a particle! Such a study has applications in crowd management.

Some of the physical properties of granular materials that are studied include force chains

– paths of (high) stress that carry a push of force into the granular material, permeability – the quality of a granular material representing the ease through which fluids can be made to pass through them, anisotropy – any directional bias in arrangement of the particles, porosity – fraction of empty spaces between the particles. It is obvious that such properties depend of the geometry of individual particles and their physical nature and the kinds of interactions between their particles. What I am interested in is to ignore all the geometrical mess and only look at the topology of a packing and see how it correlates with its physical properties. All I care about is how the particles are connected with each other, not their shape or their physical nature. Examples of objects that one studies in this direction are the Morse Smale complex, the contact network and the pore network. In this thesis, I primarily aim to study the 'duality' between the particles and these voids that exist due to their complementary nature. Further, I am interested to explore co-relations between particle and void connectivity to the physical properties of the material.

2.2 How to study them?

In order to study granular materials, one needs a way to look inside them. One popular way of doing so is to use computed tomography (CT) scans. The X-ray CT scan of a granular materials gives one a 3D scalar field image that captures how much X-ray is absorbed at a point in the illuminated region. Usually, the particles absorb X-rays and hence appear bright in the CT scan. The thicker parts of the particles absorb more X-rays than the thin parts. Of course, this depends on the nature of the particles in the material. An example is given in the figure below that shows a volume rendering of the X-ray CT of a collection of sand particles.

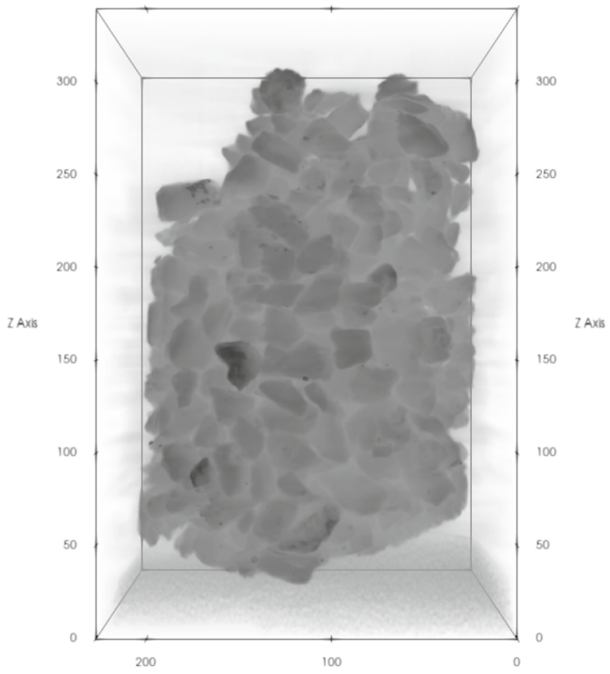

Figure 2.1: Volume rendering of CT data of sand dataset. Image taken from [23].

CT data usually also has errors in it. A particular kind of errors occur due to the tomography step and are called as *artifacts*. The figure below shows artifacts in a 2D slice of volume rendering of the sand dataset 2.1.

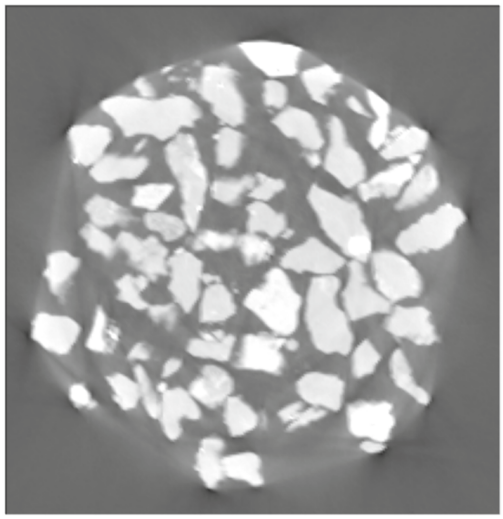

Figure 2.2: An example of artifacts in CT data. Image taken from [23].

Since we work with a 3D scalar field image of a granular material, we do not know where the particles or the voids are – we just have a scalar function created from them! Therefore, the first thing one does is to the segment the particles and the voids. Segmentation would tell you where the particles and the voids are in the 3D scalar field image of a granular material. This is not an easy thing to do just like anything where you deal with real-word data – there is always some noise in the data. Hence, the techniques adopted to perform segmentation must be resistant to errors in the 3D scalar field image as much as possible.

I explored three techniques to do segmentation. First is the good old watershed method. This is easy to implement for both particles and voids but is often error prone. So I explored *Morsegram* [23] – a Morse theory based method to segment particles and *Lovamap* [25] – a medial axis based method to segment voids. We begin by discussing application of watershed method in the context of granular materials followed by Morsegram and then Lovamap.

2.3 Watershed based segmentation

Watershed based segmentation is have been extensively used for segmenting particles in granular materials. It is known to be sensitive to noise in the data (for example, artifacts 2.2) and over segmentation of particles. Let us, however, go through a usual watershed based pipeline used for segmenting particles.

Recall from Section 1.8.3 that watershed method needs a scalar function whose extrema (either all maxima or all minima) are in one-to-one correspondence with the objects you are segmenting. To use watershed method for particle segmentation, we need to first choose such a scalar function. The most natural choice is the (inverted) distance from particle-void boundary. In principle, the particles would correspond to maxima of this distance function. But due to irregular shape of the particles (specifically non-convex shapes) and the noise in the data, practically, when one finds such a function for example using the Euclidean distance transform, one ends up with spurious maxima. If one would blindly use watershed based segmentation on such a distance function, they would end up with a lot of over-segmentation. To prevent it, one uses techniques like the h-maxima transform to suppress all the maxima with value below a specified tolerance which the user specifies. Then one inverts the field,i. e., $x \to -x$, so that the maxima become minima to apply watershed method.

Apart from the hard to fix over-segmentation of non-convex particles, other spurious maxima that are fixed using h-maxima transform require user input tolerance value but the user rarely has a meaningful choice for it. Further, small changes in h-maxima step may result in large variations in the particle segmentation. Due to these limitations, watershed bases pipelines are not preferred for particle segmentation. In the next section, we discuss a better, more robust Morse theory based segmentation pipeline [23].

2.4 Morse Theory Based Particle segmentation

In this section, we discuss the particle segmentation pipeline described in [23]. The authors propose the use of the Morse Smale complex to represent the individual particles along with their connectivity through their contact network. Further, they adopt ways to tackle noise in the data to increase accuracy of the particle segmentation. This is done using a topological persistence idea. The use of the Morse Smale complex in this setting allows it to store other data like particle-particle contact regions naturally as we will see. The final product that the authors create is called *morsegram* and has many more cool feature which we do not discuss in this thesis. We also do not go into implementation details and practical consideration because they are irrelevant for the scope of this thesis.

Actually, just the Morse complex would suffice for the purpose of particle segmentation and computation of the contact network. The authors use the Morse Smale complex because it is easier to compute. Check [28, 29] which describe this in detail. Without a way to compute the Morse Smale complex effectively, its use for segmenting particles would not be practical.

An important thing that we did not discuss in the previous section was that the quality of the particle segmentation directly depends on the quality of the particle-void interface. Many segmentation pipelines use thresholding such as Otsu's method discussed in Section 1.8.1 which find a globally optimal surface iso-surface which does not respect the local intricate geometry of particles. To fix this, the authors of [23] used Active Contours Without Edges (ACWE) method discussed in Section 1.8.1 that starts which a iso-surface created via thresholding and then goes through a series of local adjustments to create a more accurate particle-void interface.

The heart of the method is understanding the distance function from the particle-void interface from a Morse theory perspective. We do this in the section below.

Analyzing Morse Smale Complex of the Distance Function

Let f : voxels $\to \mathbb{R}$ be the signed distance from the particle-void interface computed using ACWE method described in Section 1.8.1. The distance is negative inside the void space and positive inside the particle space using Chamfer distance transform.

We expect that the local maxima of this function correspond to the particles. There is more to it. The points of contacts of the two particles would be 2-saddles! This is because the descending 3-manifolds of the maxima meet there. The ascending 1-manifold of the 2-saddles is the steepest ascend arc connecting a 2-saddle to a maximum associated with the contact particle. Look at the following figure.

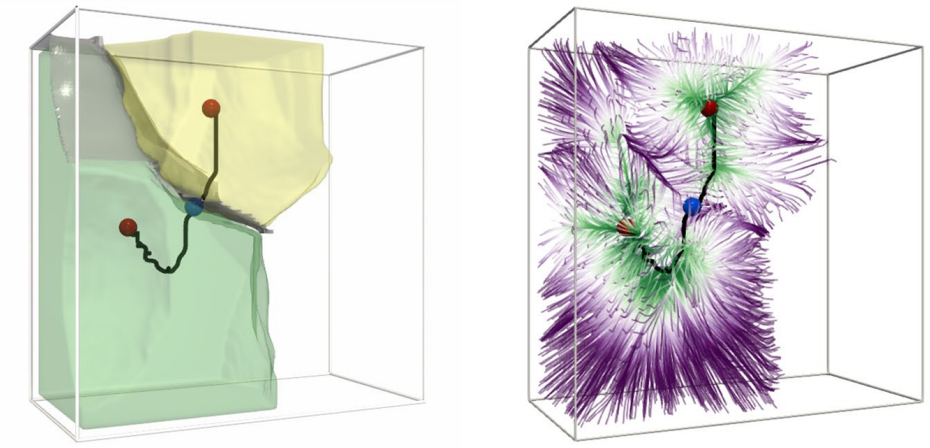

(c) **(d)**

Figure 2.3: Figure 5c and 5d from [23]. c) A pair of adjacent maxima are highlighted, their descending manifolds are shown in yellow and green. The 2-saddle at the interface of these two maxima is shown as a blue sphere. The descending manifold of this 2-saddle is the grey surface at the interface between the descending manifolds of the two maxima. The bold black line is the ascending manifold of the 2-saddle which also connects the two maxima. d) The integral lines within the descending manifolds of the two maxima. Notice how these lines converge towards the two maxima and form a separation surface around the 2-saddle.

In summary, we have the following.

1. The descending 3-manifolds of local maxima correspond to particles.
2. The descending 2-manifolds of 2-saddles (with positive distance values) correspond to contact regions.
3. The ascending 1-manifold of 2-saddles (with positive distance values) correspond to edges in the contact network.

Also, it follows from the way the distance function has been defined, and the fact that the (topological) boundary of a subset and its complement are the same, we should be able to use the Morse theory ideas to segment the voids as well. We have the following.

1. The ascending 3-manifolds of minima corresponds to voids.
2. The ascending 2-manifold of 1-saddles (with negative distance values) correspond to contact regions.
3. The descending 1-manifold of 1-saddles (with negative distance values) correspond to edges in void network.

This is same as what we had for particles but in a way we have just negated the distance function from the boundary.

The above discussion holds in an ideal world where there is no noise neither in the input data nor in created because of the pipeline used. To address these issues, we use clever topological methods described in the following subsection.

2.4.1 Topological simplification using persistence

There is always some noise in data and for segmentation problems it is usually leads to over-segmentation. Small, insignificant features that result from high frequency noise or sampling artifacts in the CT scan data lead to poor segmentation of the input granular material.

In order to tackle this, the authors used critical points pair cancellation in the MS complex they compute. This results in a simpler MS complex and Morse theory guarantees the

existence of a simpler Morse function corresponding to the simplified MS complex. The authors cancel pairs of maxima and 2-saddles because these pairs correspond to particles and its contacts as discussed above. Let p_2, q_3 be a 2-saddle and a maxima respectively. The cancellation scheme is as follows.

1. p_2, q_3 and all arcs incident on them are deleted.
2. Arcs incident on q_3 are routed to the surviving maximum connected to p_2 in the MS complex.
3. The geometry of the descending manifold of q_3 is merged into the descending manifold of of the surviving maximum that was connected to p_2.

Advantages of this method are

1. The algorithm it uses is combinatorial and therefore it does not suffer from numerical computational errors.
2. It supports controlled simplification where data outside of a local neighborhood is not affected in each iteration of the algorithm.

Note that the order of cancellation of critical point pairs matters and is important in determining the structure and geometry of the simplified MS complex. The order of critical point pair cancellation should depend on the importance/ significance of the feature that the critical point pair represents. This is judged by the difference between the function values of the critical points, also called their *persistence*. In our context, the function we are using is the distance from the boundary surface. Then the persistence of a maxima and 2-saddle is a proxy for the radius of the particle they represent. Therefore, a smaller persistence value of a maxima and 2-saddle pair means that the pair is close to each other and the particle they represent isn't significant and probably a result from artifacts in the CT scan data or over-segmentation. High persistence pairs are, therefore, correspond to particles that are 'big' in the sense that their contact points are much closer to the boundary surface than their centers.

Another important aspect to consider is the amount of simplification to be performed. The authors decide this using a *persistence diagrams* and *persistence curves*. A persistence

diagram is a scatter plot of the function values of the critical point pair. A persistence curve is a plot of the number of critical point pairs remaining against the value of the persistence. Look at the figure below for an example.

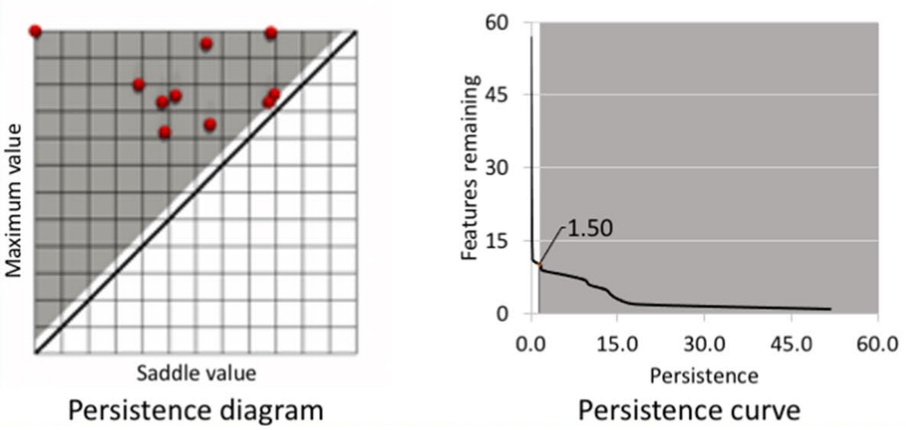

Figure 2.4: A snippet from Figure 6 from [23] showing persistence diagram (left) and persistence curve (right).

A 'knee' in the persistence curve corresponds to a critical value of the persistence that separates significant features from the insignificant ones. The authors cancel all 2-saddle maximum pair having persistence value smaller than the persistence value corresponding to the knee found from the persistence curve.

2.4.2 Implementation Details

The input CT scan data is modeled as a continuous function on 3D cube grid. The function values are defined on the vertices of the grid and interpolated in the volume of the grid. A simulated perturbation is then applied that ensures that neighboring vertices do not have same function values. This is done to ensure that the gradient is zero only at the critical points.

The boundary surface is computed and is stored at the resolution of the input CT scan. The distance from the the boundary surface field is computed and stored.

Next, the MS complex is computed using the parallel algorithm relying on graph theory described in [28, 29] that prevents inaccuracies from errors due to actual gradient computations.

Three types of manifolds are computed – descending 3-manifold of maxima, descending 2-manifold of 2-saddles and ascending 1-manifold of 2-saddles and are stored in topologically consistent manner in a unified data structure that supports fast queries. This is done by storing the connectivity of the MS complex separately from its geometry – the nodes and arcs of the MS complex is stored as a graphs and geometry is computed on demand. The MS complex contains all the information we desire along with noise. In next steps, we start interpreting the information and remove the noise.

The descending 3-manifolds corresponding to the maxima further restricted to lie within the boundary surface is the desired segmentation of the particles. This step may produce over-segmentation which is fixed using merging protocol described in Subsection 2.4.1. The persistence curve for 2-saddle maxima pairs is computed and all these pairs with persistence value less than the persistence value corresponding to the 'knee' is this curve are deleted. This procedure keeps only the significant features and gets rid of the features due to high frequency noise and artifacts in CT scan data. The authors also take into consideration another geometric finding. They observed over-segmentation in particles whose contact surfaces are much bigger than their particle sizes. To exclude such segmentation, the authors used the ratio of distance function of 2-saddle corresponding to its contact point and the maximum corresponding to the particle center. The ratio values greater than 0.75 showed over-segmentation and these pair were merged with neighboring particles.

2-saddles of the distance function with positive value represents a contact between two particles because the descending 3-manifolds of their corresponding maxima meet there.

The ascending 1-manifold of these 2-saddles is the steepest ascent arc connecting them to maxima and therefore, the collection of all ascending 1-manifolds of 2-saddles is a geometrically meaningful connectivity network. This raw connectivity network is full of spurious and clustered 2-saddles and multiple arcs connecting a pair of maxima. One needs to extract the underlying basic connectivity graph from this and delete the noisy bits. We do this by only keeping the 2-saddle with the highest function value and its arcs in the network. This 2-saddle is deemed the primary contact 2-saddle among the many 2-saddle in the contact region between two particles.

For each pair of particles, the contact regions are computed by trimming the descending 2-manifolds of the 2-saddle with highest function value to fit it into the boundary surface of material. This is done by deleting the voxels in the descending 2-manifold that have negative

distance function values.

2.5 Problems with Void Segmentation

The problem of segmenting both particles and voids of a granular material is of great importance because the properties of the material depend on how its particles and voids are arranged. Voids in granular material form naturally – when multiple particles of different shapes come close they do not interlock but have gaps between them which we call voids. The particle space has been extensively studied, primarily because it is easier to study them – particles are discrete and can be identified relatively easily. The voids, however, are more 'continuous' and 'smeared out'. The literature on granular materials reflects a favoring towards the study of granular materials from the perspective of their particles. There is much more literature from perspective of particles in granular materials than the perspective of their voids. For many applications, local information about the voids is more important – for example landslide and earthquake science and bioengineering.

Some of the pervious work in this direction includes the use of Delaunay triangulation and Voronoi tesselation but these methods suffer from over-segmentation problems.

In the next section, we discuss [25], which is an attempt to meaningfully segment the void space of a granular ensemble and understand the voids in granular materials locally. In order to do this, [25] employs a sequence of very clever steps that requires significant wisdom to come up with. We discuss this in the next section.

2.6 Medial Axis Based Void segmentation

In this section, we discuss the void segmentation pipeline described in [25]. The final product that the authors create is called *lovamap* which stands for **Lo**cal **V**oid **A**nalysis using **M**edial **A**xis by **P**article configuration.It has many more cool feature which we do not discuss in this thesis. We also do not go into implementation details and practical consideration because they are irrelevant for the scope of this thesis. We start by discussing the medial axis transform the way it is used in [25].

2.6.1 Medial Axis Landmarks

The medial axis of a subset of a space, as discussed in Section 1.4.3, is the set of points having at least one closest point on the object's topological boundary.

In [25], the authors use the following terminology for medial axis of the particle space. They call the set of points equidistant from exactly 2 particles a *2D ridge* since it is a surface. The intersection of two 2D ridges is called a *1D ridge* since its a curve. Note that a 1D ridge consists of points that are equidistant to either 3 or 4 particles. Finally, intersection of 1D ridges is called a *peak*. Note that a peak is equidistant to at least 4 particles and it corresponds to a local maxima in the euclidean distance transform of the particle boundary.

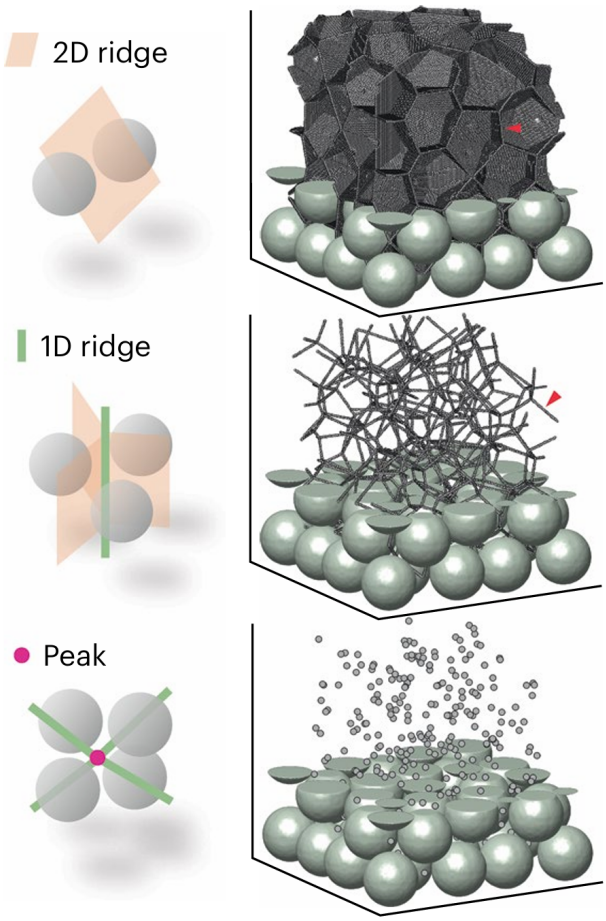

Figure 2.5: Medial axis subtypes that lovamap defines as spatial landmarks. Figure 1e from [25]

Next, we discuss five things that set lovamap apart.

2.6.2 Distinguishing Features of Lovamap

The following clever features are the reason why the void segmentation done by lovamap is superior.

EDT computed for every particle

In order to compute the medial axis, usually one does so using the boundary of the particles. We compute the Euclidean distance transform from the boundary of the particles and then look at points that are equidistant from the boundary. This has several problems due to noise in the particle data. For example, one gets 'hairy branches'.

Instead, lovamap computes the Euclidean distance transform from every particle and stores it separately. This allows it to store both which points are equidistant to the particles and equidistant to exactly what particles. This immediately fixes the above mentioned issue of 'hairy branching' of medial axis near a non-convex shaped particle.

Medial axis is computed using a very systematized approach

Classic methods for finding the medial axis include morphological approaches like erosion algorithms, dilation algorithms, crash detection in wave propagation and trying to fit maximal spheres inside the void space. These methods work but have a major accuracy problem.

Lovamap uses a very ingenious way to find the medial axis that exploits the particle configuration itself. This approach is called *MAPC – medial axis by particle configuration*. As discussed in Section 2.6.1, 2D ridges, 1D ridges and peaks are defined and their points are labeled with an id relating to the particles that are equidistant from the points. For example, points in the 2D ridge equidistant to particles A and B are is labeled with id (A, B). This technique makes lovamap very particle centric and restricts its use only to granular materials in which the particle segmentation is known.

Neighbouring-particles network of particles is used to determine parts of medial axis

Using the medial axis, the authors try to capture the connectivity of the particles using a graph that they call the 'neighbouring-particles network'. The vertices of this graph are the particles themselves and there is an edge between two particles if there is a point in the void space equidistant from the two particles.

The authors make the key observation that the set of smallest loops in this graph defines all unique 1D ridges in the particle system. This idea is demonstrated in the following image.

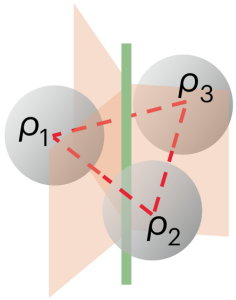

Figure 2.6: Figure 1f from [25]: A 1D ridge loop demonstrates the idea that smallest loops in neighbouring-particles network correspond to 1D ridges.

The authors first find the set of smallest loops in the neighbouring-particles network and use them to find the 1D ridges. This guarantees the existence of 1D ridges – one does not need to search through the entirety of points in the void space but a small subset. This would be elaborated in the next section.

No over segmentation due to multiple peaks

We could identify peaks more tangibly like we identified 1D ridges using the neighbouring-particles network. We would need to find the set of smallest polyhedron in the neighbouring-particles graph, however, this is a difficult algorithmic problem that is not solved yet. Instead, we use a very neat heuristic to club peaks together. Two peaks are clubbed together if the distance between them is smaller than the sum of their radii. For more details, check the next section.

Voids' entrance and exit are captured

Lovamap went above and beyond the void space segmentation game. Not only it meaningfully segments the voids it also captures the entrance and exits of voids into the granular material and how voids move around in the interior.

To capture the entrance and exit of voids, lovamap separately segments the outer boundary of the granular material and then combines it with the segmented voids later.

2.6.3 Implementation Details

Lovamap takes as input an 3D image made of voxels and labels the voxels that describe a particle with that particle's id. This is how lovamap stores the granular material. Without loss of generality, the authors decided to work with mesh size on the scale of micrometers.

To compute the Euclidean distance transform for each particle, lovamap first 'smooths out' each particle by using a threshold of $\sqrt{2}$ times the mesh size to determine the boundary surface of the particle. The Euclidean distance is then computed with respect to this surface of the particle. Also, since granular materials have a very large number of particles, it is very difficult to store the entire Euclidean distance transforms for all particles. But since lovamap would only look at voxels equidistant from particles, the entire Euclidean distance transform need not be computed and stored. Lovamap first computes the Euclidean distance transform for the boundary surface of the particle space and then finds the maximum value a voxel attains. Call this value d_{max}. Then the Euclidean distance transform for each particle is only computed for voxels inside an axis aligned box of centered at the particle and extending d_{max} in all the 6 coordinate directions.

Once the Euclidean distance transforms are computed, the information about equidistant voxels from particles is stored in a sparse boolean matrix as follows. (i, j)th entry of the matrix is true if and only if the ith particle is equidistant to jth voxel. Let us call this matrix M. The sparse matrix data structure does not allot memory for the entries of the matrix that are false and hence saves a ton of memory. In practice, the authors say that a column usually has at max 10 true entries. From the matrix M, it is easy to compute the medial axis – it is collection of voxels whose corresponding columns in M have at least 2 entries as true.

Next, the voxels in the medial axis are identified. A voxel in the medial axis is labeled by the particles it is equidistant to, as mentioned before. Voxels are categorized as either a 2D ridge voxel, a 1D ridge voxel or a peak voxel. Every voxel is characterized in exactly one of the above medial axis subtypes. First, the 2D ridge voxels are identified. This is done by simply searching for columns in the M that have exactly 2 true entries. Next, 1D ridge voxels are identified using the neighbouring-particles graph as discussed in previous section – 1D ridges lie within the smallest cycles in the neighbouring-particles graph. To find them, a clever algorithm is used. Once we know the smallest cycles, finding 1D ridge voxels is a simple search in the matrix M – we search the columns that have the entry true in the rows corresponding to the particles in a smallest cycle. Lastly, to find peaks, we mine the remaining voxels in the medial axis computed before. We first cluster them using a connected components approach. In each cluster, we find the voxels that are equidistant to maximum number of particles since these voxels are better candidates for peaks. Within these voxels, we look at the voxel with the maximum Euclidean distance transform value. This voxel is our peak. Once this voxel is identified, the remaining voxels in the cluster are assigned to appropriate 1D ridges.

Once we have identified the peaks and 1D ridges, we force them to have a graph structure. Such a graph would capture the landscape of the void space. This is done in the following way – all 1D ridges that lie in the interior of the void space have a peak at both ends, the 1D ridges that extend to the boundary of the granular material have a peak at the end that lies in the interior of the void space. There are even some cases where both ends of a 1D ridge extend to the boundary of the granular material. We ignore such ridges in our ridge-peak graph. The actual way by which the authors create this graph is very involved and is built to robustly cover all possible scenarios and I do not cover it here.

Lovamap also finds 'doors' in the void space that are essentially narrow surfaces that separate two different pores from each other. To find the doors, we find the narrowest point along a 1D ridge, we search for the voxel along the ridge that has the smallest EDT value, say d_{min}. We then identify the three closest particles to the 1D ridge, and for each particle, we locate the particle voxel, v_1, v_2 and v_3, that lies closest to d_{min}. The door is then generated by fitting a circle to v_1, v_2 and v_3.

Next, lovamap associates peaks that belong to the same open space. This is done using a genius heuristic described in the below figure. The advantage to this approach is that this

approach does not require any user threshold inputs.

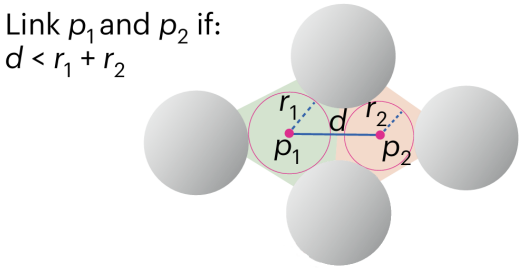

Figure 2.7: Two peaks are associated if the distance between them is smaller than the sum of their corresponding radii. Figure 1g (top) from [25].

Now that we have more natural pores after associating peaks that belong to the same open space, we find the backbone of each pore. The backbone is simply the part of the 1D ridge inside a pore. For 1D ridges that have doors through them, parts of them are allotted to corresponding pores.

Finally, using the backbone of the void space created above, pores are created using nearest-neighbors algorithm. The pores get filled starting from the backbone described above.

Once the pores in the interior of the granular material are segmented, lovamap then segments the boundary of the granular material as a separate entity using pretty much the same pipeline. Then, the boundary surface pores which share voxels with the interior pores are kept, the other boundary pores are ignored.

The authors use lovamap to analyse a lot of datasets and present very interesting statistics. They do this robustly using appropriate statistical tests wherever needed. I only present the their results and not the tests they used to make conclusive claims.

We also discussed in Section 2.4 that the ascending 3-manifolds of minima corresponds to voids, the ascending 2-manifold of 1-saddles (with negative distance values) correspond to contact regions and the descending 1-manifold of 1-saddles (with negative distance values) correspond to edges in void network. Therefore, one can also segment the void using morsegram. The segmentation produced by morsegram and lovamap are yet to be compared.

2.7 Physical properties of Granular materials

2.7.1 Porosity

Porosity is simply the void volume fraction in a granular material, i. e., ratio of volume of void space to volume of the granular material. Porosity does not tell anything about the structure of the granular material. Many different granular materials can have same porosity.

Studying porosity might be of interest. For example, the granular material where particles are humans, we do not want stampeding to happen. Empirical studies show that the porosity of this material needs to be low enough to mitigate stampeding. For example, according to [10], the safe porosity should be around 4 humans per square meter.

2.7.2 Permeability

The (absolute) *permeability* of a granular material is a measure of the characteristic of the material packing that captures the ease through which fluid can be made to pass through it.

[1] gives an mind-bending connection between the max-flow min-cut theorem in graph theory and the permeability of a granular material. Their method involves modelling the void space of a material using the void network with weights decided by Darcy's law and the Hagen-Poiseuille equation. The permeability calculated using their method based on max-flow min-cut agrees with the permeability calculated using modeling flow in the void space for permeability values spanning 5 orders of magnitude with average error around 25%.

2.8 An attempt to model granular materials

In this section, We try to give a definition for granular materials from the point of view of pure topology. Before we do that, we first make an argument that the shape of the container that holds the particles can be ignored for the purpose of this thesis. This is because the container has no role other than to hold the particles. From mathematical point of view, we can fix the particles as they are in the container and get rid of it. Obviously, this does not

limit the different possibilities of a granular material. Given any arrangement of particles. we can imagine a container around it. Therefore, we can ignore the container. Next, we define a particle.

Definition 2.8.1. *A* ***particle*** *is a subset of* $\mathbb{R}^n$ *homeomorphic to the closed* n*-ball* $\mathbb{B}^n = \{x \in \mathbb{R}^n \mid ||x|| \leq 1\}$*. Further, we require complement of each particle (in isolation) to be simply connected to rule out pathological examples like Alexander horned ball. Usually we take* $n = 2, 3$*.*

Now, we give the definition of granular materials that we will use in this thesis.

Definition 2.8.2. *A* nD granular material *is a pair* (P, V) *where* P *is a bounded subset of* $\mathbb{R}^n$*, called the* particle space*, which has a decomposition as union of finite number of particles.* V *is the complement of* P *in* $\mathbb{R}^n$ *and is called the* void space*.*

We will only deal with granular materials in dimensions 2 and 3.

Remark 2.8.1. *Obviously the definition is far too general and includes pathological examples like Alexander horned ball. We want to keep the definition restricted enough to only include physical granular materials and at the same time general enough to explore the usefulness of results from topology. We will later try out giving some more structure to* P *such that assuming that it is a handlebody, etc.*

We further assume that P does not have any torsion, i. e., its homology and cohomology groups are free.

Definition 2.8.3. *Given a granular material* (P, V)*, the topological boundary of* P *is called the* particle-void interface*. It will be denoted by* B*.*

Note that in $3D$ granular materials, the particle-void interface can have different connected components. Each of the components is compact. If B is a manifold, then by using the classification theorem for surfaces, we know that each component is homeomorphic to a genus g surface. In 2D granular materials, the particle-void interface has connected components that are homeomorphic to S^1.

Lastly, we define the contact network and the void network.

Definition 2.8.4. *Given a granular material $G = (P, V)$ with P consisting of particles $P_1, P_2, \ldots, P_n$, the* contact network *is a graph with a vertex v_k corresponding to each particle P_k and an edge (v_a, v_b) is $P_a \cap P_b \neq \emptyset$.*

Similarly, if a segmentation of the void space is given, we can similarly define a void network analogously.

Remark 2.8.2. *Note that if all triples $P_i \cap P_j \cap P_k = \emptyset$, then the contact network is the same as the nerve of $P_1, P_2, \ldots, P_n$.*

This happens for instance, when the particles are rigid and do not deform.

Part II

Results and Future Directions

Chapter 3

Applying Alexander Duality to Granular materials

In this chapter, we explore the use of Alexander duality for $\mathbb{R}^n$ 1.6.3 in granular materials. We first start with 2D materials because they are relatively simpler, and then we move on to 3D materials.

3.1 2D materials

Let us first understand what features the homology groups would capture in the context of granular materials. For a 2D granular materials $G = (P, V)$, we need to only consider $\mathrm{H}_0(P)$, $\mathrm{H}_1(P)$, $\mathrm{H}_0(V)$ and $\mathrm{H}_1(V)$. The zeroth homology group captures connected components and therefore,

1. $\mathrm{H}_0(P)$ contains a generator for each connected component of P, a *lump of particles* so to speak.
2. $\mathrm{H}_0(V)$ contains a generator for each connected component of V, a cluster of *isolated voids* so to speak.

The first homology group captures loops and therefore,

1. $\mathrm{H}_1(P)$ contains a generator for each loop in P, i. e., a collection of particles that are in contact in a way that they form a *necklace* so to speak.

2. $\mathrm{H}_1(V)$ contains a generator for each loop in V, i. e., a *closed tunnel* so to speak.

The following 2D granular material is generated using Porespy, [9] (more details in Section 3.3).

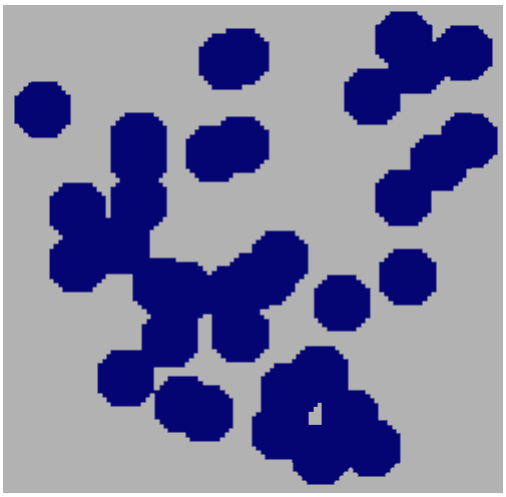

Figure 3.1: A granular material generated using Porespy [9]. The particle space is in color blue and the void space is in color grey.

Note that we have defined in Section 2.8 that the void space is the complement of the particle space in $\mathbb{R}^2$, Obviously we cannot visualize all of $\mathbb{R}^2$ on this page and hence only draw a part of it just around the particle space.

In the next figure, we highlight the features described above in this 2D granular material.

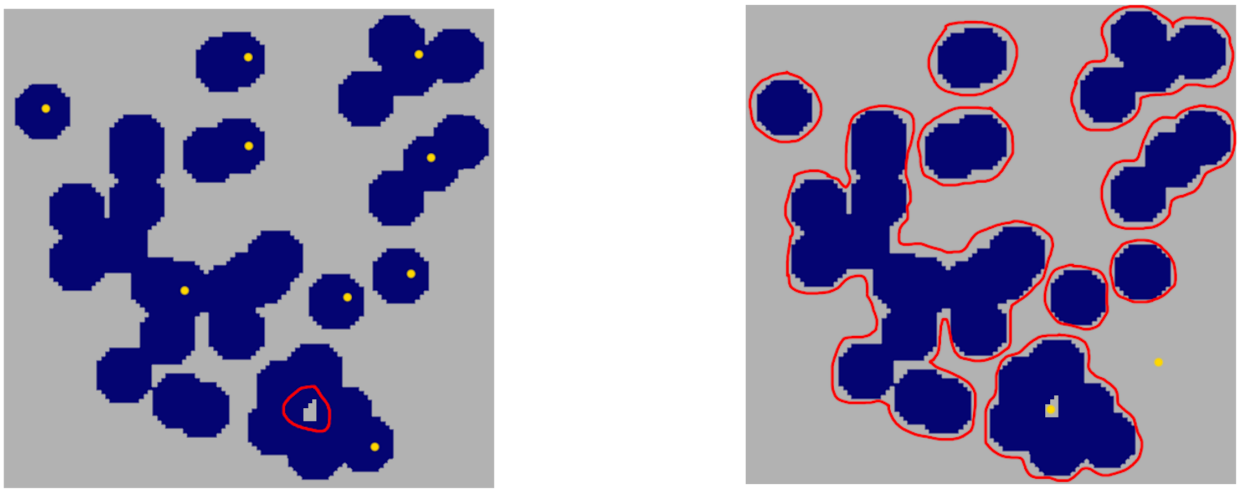

Figure 3.2: Red loops capture generators of first homology group, Yellow dots capture the connected components. Left image shows featured for the particle space (blue) and right picture shows features for the void space (grey).

In the above example 3.2, we have $\beta_0(P) = 9$, $\beta_1(P) = 1$, $\beta_0(V) = 2$ $\beta_1(V) = 9$. Note that $\beta_0(V) = \beta_1(P) + 1$ and $\beta_1(V) = \beta_0(P)$. These are precisely Equations 1.6. Now, we present the general results.

We assume that P is locally contractible and compactness of P follows because it is a finite union of compact spaces (the particles). Therefore, using Theorem 1.6.3 gives us Equations 1.6 with A replaced with P:

$$\begin{aligned} \mathrm{H}_0\left(\mathbb{R}^2 \setminus P\right) &= \mathrm{H}_0(V) \cong \mathrm{H}^1(P) \oplus \mathbb{Z} \\ \mathrm{H}_1\left(\mathbb{R}^2 \setminus P\right) &= \mathrm{H}_1(V) \cong \mathrm{H}^0(P) \end{aligned}$$

Since, by assumption, P does not have torsion, the homology and cohomology groups are the same and we have

$$\begin{aligned} \mathrm{H}_0(V) &\cong \mathrm{H}_1(P) \oplus \mathbb{Z} \\ \mathrm{H}_1(V) &\cong \mathrm{H}_0(P) \end{aligned}$$

Note that these isomorphisms can be thought of as linking between the generators of homology groups.

The above formulas simply tells us that the connected components of a subspace create loops in the complement space and loops in a subspace create connected components in the complement space[1]. In context of granular materials, we can re-frame these isomorphisms as follows:

1. Isolated lumps of particles create void tunnels around them.
2. A necklace of particles bounds an isolated void, there is an additional connected component of the void space which is the unbounded compound of the void space.

Next, we move on to the 3D granular materials case.

3.2 3D materials

We will follow same flow as we did in the previous section, we will start by discussing features that the homology groups would capture in the context of granular materials. For a 3D granular materials $G = (P, V)$, we need to only consider $\mathrm{H}_0(P)$, $\mathrm{H}_1(P)$, $\mathrm{H}_2(P)$, $\mathrm{H}_0(V)$, $\mathrm{H}_1(V)$ and $\mathrm{H}_0(V)$. The zeroth homology group captures connected components and therefore,

1. $\mathrm{H}_0(P)$ contains a generator for each connected component of P, a lump of particles so to speak.
2. $\mathrm{H}_0(V)$ contains a generator for each connected component of V, a cluster of isolated voids so to speak.

The first homology group captures loops and therefore,

1. $\mathrm{H}_1(P)$ contains a generator for each loop in P, i. e., a collection of particles that are in contact in a way that they form a *necklace* so to speak.
2. $\mathrm{H}_1(V)$ contains a generator for each loop in V, i. e., a *closed tunnel* so to speak.

[1]This is akin to the complement of a graph in $\mathbb{R}^2$ example we discussed 4.

The second homology group captures cavities and therefore,

1. $\mathrm{H}_2(P)$ contains a generator for each *cavity* in P, i. e., a collection of particles that are arranged in a way that they isolate a void inside them so to speak. Usually, this results from cavities inside the particles themselves or through good contact between non-convex particles.
2. $\mathrm{H}_2(V)$ contains a generator for each *shell* in V, i. e., void space surrounding a lump of particles so to speak.

Unfortunately, it is incredibly hard to get nice example for 3D material case unlike the example we presented for the 2D material case. We would need to rely on our imagination here. We give the final result now.

We assume that P is locally contractible and compactness of P follows because it is a finite union of compact spaces (the particles). Therefore, using Theorem 1.6.3 gives us Equations 1.6 with A replaced with P:

$$\begin{aligned}
\mathrm{H}_0\Big(\mathbb{R}^3 \setminus A\Big) &= \mathrm{H}_0(V) \cong \mathrm{H}^2(A) \oplus \mathbb{Z} \\
\mathrm{H}_1\Big(\mathbb{R}^3 \setminus A\Big) &= \mathrm{H}_1(V) \cong \mathrm{H}^1(A) \\
\mathrm{H}_2\Big(\mathbb{R}^3 \setminus A\Big) &= \mathrm{H}_2(V) \cong \mathrm{H}^0(A)
\end{aligned}$$

Since, by assumption, P does not have torsion, the homology and cohomology groups are the same and we have

$$\begin{aligned}
\mathrm{H}_0(V) &\cong \mathrm{H}_2(A) \oplus \mathbb{Z} \\
\mathrm{H}_1(V) &\cong \mathrm{H}_1(A) \\
\mathrm{H}_2(V) &\cong \mathrm{H}_0(A)
\end{aligned}$$

Note that these isomorphisms can be thought of as linking between the generators of homology groups.

In the context of granular materials as discussed above, we can re-frame these isomorphisms as follows:

1. Isolated lumps of particles create void shell around them.

2. A necklace of particles links with a tunnel in void space.

3. A cavity creates a connected component of the void space. There is an additional connected component of the void space which is the unbounded compound of the void space.

3.3 Computational Experiments

As a first step in validating Theorem 1.6.3, we tried some computational experiments using python libraries Gudhi (in particular, cubical complex [5] in Gudhi was used) and Porespy[9]. The code was written using Google Gemini and is available along with the materials that were generated using it here: https://github.com/HeerakSharma/PoreSpy_Materials_Betti_Numbers.

Porespy is a python library that generates random particles in a specified voxel domain with specified parameter values like porosity, radius of spheres, etc. There are three types of particles shapes one can generate: spheres, blobs and cylinders. We generated materials using the 'spheres' and 'blobs' methods and did not use the 'cylinders' method due to runtime errors. In order to be general, we chose to work with materials with a variety of parameter values. Specifically, we generated materials of size $50 \times 50 \times 50$ voxel^3 for porosity values $0.1, 0.2, 0.3, 0.4, 0.5, 0.6, 0.7, 0.8, 0.9$. For each porosity value, if we generated materials using method 'blobs' then we generated 10 materials each for blobiness values $0.5, 1.5, 2.5$; if we generated materials using method 'spheres' then we generated 10 materials each for radius values $5, 10, 15, 20, 25, 30, 35, 40, 45$.

Computing Betti numbers of the materials was done using Gudhi as mentioned previously. There was as slight nuance to this. Directly finding Betti numbers of materials generated by the above described scheme has two problems.

1. If we want to test 1.6.3 for granular materials, then we need to center the materials generated using PoreSpy so that they can be modeled as materials in $\mathbb{R}^3$ without their container. This is done by padding the numpy array representing the material.

2. Correct connectivity is crucial. Connectivity problems occur when processing the materials generated by PoreSpy. An example of the problem is given below for a 2D material.Consider a 2×2 pixel space X in which the $1, 1$ and $2, 2$ pixels forms a subspace A. Since the $1, 1$ and $2, 2$ pixels intersect with each other at the center of the space X, A is connected subset of X and $X \setminus A$ is has two connected components. But Gudhi treats the two connected components of $X \setminus A$ as being a single component. This would obviously cause errors in the computation of Betti numbers.

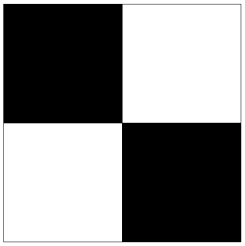

Figure 3.3: Figure showing 2×2 pixel grid where the $1, 1$ and $2, 2$ form the space A.

Similar problems also happen with 3D complexes but are hard to show with pictures.

To fix these problems, the following scheme is used. First, note that these problems are possible to occur whenever a particle voxel is adjacent to a void voxel. To fix such problems, we can just add a little more material to the contact region of the particle voxel and the void voxel. This is implemented using a brute-force scheme as follows. We first subdivide each voxel into 8 sub-voxels in the obvious way. If a particle voxel has a void voxel on its left, then rightmost face comprising of void sub-voxels in contact with the particle voxels is converted into particle sub-voxels. Once this is done for all voxels, the same thing is repeated not along the top-bottom axis instead of the left-right axis. Each sub-voxel is further subdivided into 8 sub-sub-voxels. If a particle sub-voxel has a void sub-voxel on its top, then the bottommost face comprising of the void sub-sub-voxels is converted into particle sub-sub-voxels.

As illustrated above, each material generated using PoreSpy was pre-processed to fix the above described problems. Then, Gudhi was used to compute Betti numbers of the void space and the particle space. For all of the generated materials, the Betti numbers of the particle space and void space follow Formulas 1.6.

Chapter 4

Contact Network and Pore Network

This chapter explores some ideas based on the contact network and the void network. We discuss a connection between average coordination number of particles in a granular material and the first Betti number of its particle (or void) space.

4.1 Exploring the contact network

In this section, we explore the contact network further. We present relationships between the coordination numbers of a granular material, in particular the average coordination number, with the first Betti number of the particle and the void space. At last, we also explore what happens locally in the void space around a particle.

4.1.1 Some graph theory stuff

First Betti number and first handshaking lemma

Let G be a graph with $\mathfrak{v}$ vertices, $\mathfrak{e}$ edges and $\mathfrak{c}$ connected components. Let Ver denotes the vertex set of the graph and for $v \in \text{Ver}$, $d(v)$ denote the degree of the vertex v. Recall from Section 1.1 that the first Betti number of a graph is given by $\beta_1(G) = \mathfrak{e} - \mathfrak{v} + \mathfrak{c}$.

We can use the first handshaking lemma to express e in terms of the degree of vertices in G. Recall that the first handshaking lemma states that

$$\sum_{v \in \text{Ver}} d(v) = 2\mathfrak{e}.$$

We can use this to express $\mathfrak{e}$ as $\frac{1}{2}\left(\sum_{v \in \text{Ver}} d(v)\right)$. This gives the following formula for $\beta_1(G)$

$$\beta_1(G) = \frac{1}{2}\left(\sum_{v \in \text{Ver}} d(v)\right) - \mathfrak{v} + \mathfrak{c} = \frac{1}{2}\sum_{v \in \text{Ver}} (d(v) - 2) \ + \mathfrak{c}. \tag{4.1}$$

Formula (4.1) gives us a way to think of $\beta_1(G)$ in terms of how connected vertices each vertex is which is captured by the degree of vertices of the graph. We discuss two primitive examples below.

Example 5. *1. Let G be graph with each connected component a vertex or an edge. The degree sequence of such a graph is $(0, 0, \ldots, 0, 1, 1, \ldots, 1)$. The first term in (4.1) precisely equals $-\mathfrak{c}$ making $\beta_1(G) = 0$.*

2. Let G be a graph with each connected component a cycle. The degree sequence of G is $(2, 2, \ldots, 2)$ and therefore, the first term in (4.1) vanishes and we are $\beta_1(G) = \mathfrak{c}$ meaning each cycle in G contributes 1 in the first Betti number of G.

Average degree and first Betti number

We can also express Formula (4.1) in another form

$$\beta_1(G) = \mathfrak{v}\left(\frac{1}{2}\left(\sum_{v \in \text{Ver}} d(v) \Big/ \mathfrak{v}\right) - 1\right) + \mathfrak{c} = \mathfrak{v}\left(\frac{\overline{d}}{2} - 1\right) + \mathfrak{c} \tag{4.2}$$

where $\overline{d} = \sum_{v \in \text{Ver}} d(v) \Big/ \mathfrak{v}$ is the average degree of a vertex.

Equation (4.2) tells us that there is a nice relationship between the first Betti number of a graph G in terms of its average degree and number of vertices. For a fixed $\mathfrak{v}$, $\beta_1(G)$ grows linearly with $\overline{d}$ which makes sense – the lower the $\overline{d}$, the sparser the graph G and the lesser

chance of there being many independent cycles in G.

Looking locally around a vertex

Lastly, we discuss what happens locally at a vertex v in a graph G with respect to the first Betti number. For $v \in \mathrm{Ver}$, let $\mathrm{N}(v)$ denote the collection of vertices adjacent to v. The vertices in $\mathrm{N}(v)$ can have edges between them. These edges are what give rise to generators in $\mathrm{H}_1(G)$. Take a look at the following figure.

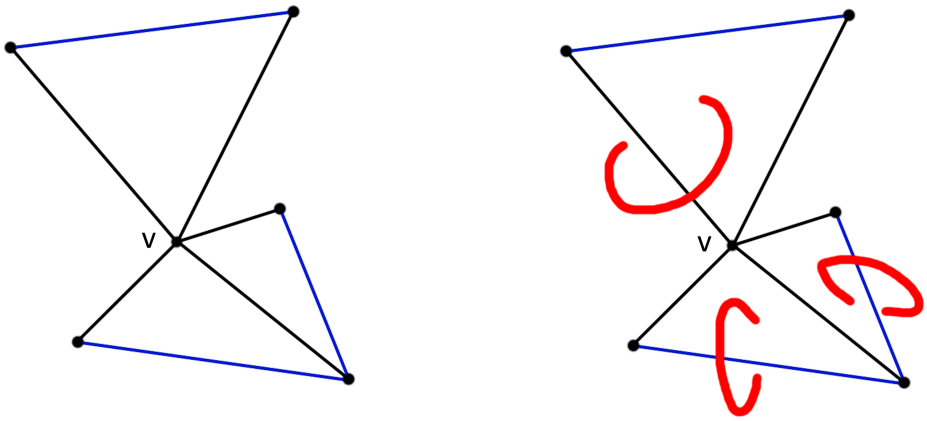

Figure 4.1: Left: The neighborhood of a vertex v in a graph G with edges between the neighbor vertices shown in blue. Right: The generators of $\mathrm{H}_1(\mathbb{R}^3 \setminus G)$ locally around the vertex v.

Each edge between vertices in $\mathrm{N}(v)$ completes a triangle with v as one of the vertex. Each such triangle corresponds to a generator of $\mathrm{H}_1(\mathbb{R}^3 \setminus G)$ passing through each such a triangle. This idea of generators of the complement "passing through" a triangle can be generalized and we will briefly discuss them in Section **??**.

Note that these generators are not the only generators for $\mathrm{H}_1(\mathbb{R}^3 \setminus G)$ and not all generators of $\mathrm{H}_1(\mathbb{R}^3 \setminus G)$ can be obtained through this way.

4.1.2 What this means for granular materials?

Now, we see the consequences of Equation (4.2) in the context of granular materials. This would be done through application of the discussion in Section 4.1.1 to the contact network of the granular material defined in Section 2.8.4.

First, degree of a vertex in the contact network is the coordination number of the particle corresponding to the vertex in the particle space. Therefore, Equation (4.2) is a connection between the average coordination number in a granular material and the first Betti number of its contact network.

Recall from Remark 2.8.2 that if the intersection of no three particle is non-empty, then due to Leray's nerve theorem 1.2.1, the contact network is homotopy equivalent to the particle space. This happens for instance, when the particles are rigid and do not deform.

In such cases, have a connection between the average coordination number and the first Betti number of the particle space. Since Alexander duality tells us that the first Betti number of the particle space equals the first Betti number of the void space as discussed in Section 3.2, the average coordination number of the particles tells us about the first Betti number of the void space. We state this result formally below.

If d is the average coordination number of particles in a granular material, then the first Betti number of the particle space and the first Betti number of the void space is $n(\frac{d}{2} - 1) + c$ where n is the number of particles in the material and c is the number of connected components in the particle space of the material.

This can be sometimes useful. This is because sometimes one knows an estimate for the average coordination number in a granular material and then one can translate that to an estimate on the first Betti number of the particle space (or the void space) of the granular material. For example, Appendix A in [2] discusses theoretical bounds on coordination number for random packings of frictionless and frictional particles in m dimensions that satisfy periodic boundary conditions using Maxwell counting arguments. The materials we discuss in this thesis are in $\mathbb{R}^3$ and they do not satisfy periodic boundary conditions. But, we believe that the estimates are still good since the number of particles on the boundary of the container are much less than the number of particles in the bulk of the material. In 3D, we have

1. For frictionless particles, average coordination number is 6. Using (4.2), we have that the first Betti number is close to $2n + c$ where n is the number of particles and c is the number of connected components in the particle space.

2. For frictionless particles, average coordination number $d \in [4, 6]$ Using (4.2), we have that the first Betti number roughly lies in the interval $[n + c, 2n + c]$ where n is the number of particles and c is the number of connected components in the particle space.

An important question is that are Betti numbers physically relevant? There is some evidence that they are. [15, 16] introduce the use of Betti numbers to quantify the number of connected components and loops in force networks, demonstrating how topological invariants evolve under compression.

4.1.3 What happens locally around a particle?

As the last thing in this section, we translate the discussion in Section 4.1.1 to the context of granular materials. This boils down to the following. Each triangle a particle is part of corresponds to a generator of the first homology group of the void space. AS discussed in Section 4.1.1, these generators are not the only generators for the first homology group of the void space and not all generators of the first homology group of the void space are obtained through this way.

Chapter 5

Other Directions Explored

5.1 Using Handle-bodies in granular materials

5.1.1 What is a Handlebody?

Given an n-manifold M with boundary ∂M, adding an *handle* to M is a specific way of gluing an n-ball B^n to M determined by how one glues parts of the boundary of $\partial B^n = S^{n-1}$ to M. Note that for each $k \in \{0, 1, 2, \ldots, n\}$, $B^n = B^k \times B^{n-k}$ and hence, $\partial B^n = \partial B^k \times B^{n-k} \cup B^k \times \partial B^{n-k} = S^{k-1} \times B^{n-k} \cup B^k \times S^{n-k-1}$. To add a k-handle to M, one glues $S^{k-1} \times B^{n-k}$ to ∂M, i. e., $S^{k-1} \times B^{n-k}$ is identified with a subset of ∂M, and we let everything else be as it is. After this gluing, $(M, \partial M)$ transforms into $(M', \partial M')$ where $M' = M \cup B^n$ and $\partial M' = (\partial M \setminus S^{k-1} \times B^{n-k}) \cup B^k \times S^{n-k-1}$.

An *n-dimensional k-handlebody* is a space constructed from gluing l-handles to B^n for $l \leq k$. Note that one can glue handles in different ways resulting in different spaces. But all of them are homeomorphic.

We are particularly interested in 3-dimensional 1-handlebodies. The reasons are

1. 3-dimensional 1-handlebodies are "thickenings" of graphs,

2. under some assumptions, the particle space is a handlebody.

Lemma 5.1.1. *Let G be a finite, connected graph. The closed regular neighborhood of G is a 1-handlebody.*

Next, we discuss [30], which studies piecewise-linear embeddings of 3-dimensional 1-handlebodies in S^3. The reason for studying this paper was to understand basic properties of 3-dimensional 1-handlebodies and explore their use in granular materials. The main motivation was to explore if knots in a granular material would be of any significance. The author is still thinking about this.

5.1.2 Suziki's paper

The paper [30] classifies piecewise-linear embeddings of graphs seen as 1-dimensional simplicial complexes in the 3-sphere. We start with a few definitions.

Let K denote the set of all connected finite 1-dimensional simplicial complexes. For an element $G \in K$, we call $(G \subset S^3)$ a *graph* in S^3. Let $K(n)$ denote the subset of K with first Betti number n. Let H denote the collection of all 3-dimensional 1-handlebodies. For an element $T \in H$, we call $T \subset S^3$ a handlebody in S^3. Let $H(n)$ denote the subset of H of genus n. Note that the embeddings $G \subset S^3$ and $T \subset S^3$ are in general knotted,i. e., there are cycles in them that are non-trivial knots. The goal of the rest of this section is to understand the structure of these embeddings.

For a pair $(P \subset M)$, $\mathrm{N}(P; M)$ denotes the regular neighborhood of P in M. We give two notions of equivalence of two embeddings below.

Definition 5.1.1. *Two pairs $(P_1 \subset M_1)$ and $(P_2 \subset M_2)$ are said to be* equivalent*, denoted by $(P_1 \subset M_1) \sim (P_2 \subset M_2)$ if there is a homeomorphism $h : M_1 \to M_2$ such that $h(P_1) = P_2$. Further, h is orientation preserving if M_1 is oriented.*

It is clear from the above definition of equivalence of pairs that $\sim$ is an equivalence relation. We denote the equivalence class of a pair $(P \subset M)$ by $< P \subset M >$. For graphs $G \subset S^3$, their equivalence class is called a *graph type*. Next, we give a notion of equivalence of two neighborhoods.

Definition 5.1.2. *Two pairs $(P_1 \subset M_1)$ and $(P_2 \subset M_2)$ are said to be* neighborhood equivalent*, denoted by $(P_1 \subset M_1) \overset{N}{\sim} (P_2 \subset M_2)$, if $(\mathrm{N}(P_1; M_1) \subset M_1) \sim (\mathrm{N}(P_2; M_2) \subset M_2)$.*

It follows from uniqueness of regular neighborhoods **??** that the above definition does not depend on the either the regular neighborhoods $\mathrm{N}(P_1; M_1)$, $\mathrm{N}(P_2; M_2)$ or the triangulations of M_1 and M_2.

Note that $\overset{\mathrm{N}}{\sim}$ is an equivalence relation. Further, if $(P_1 \subset M_1) \sim (P_2 \subset M_2)$ then $(P_1 \subset M_1) \overset{\mathrm{N}}{\sim} (P_2 \subset M_2)$. Hence, $\overset{\mathrm{N}}{\sim}$ can be defined on the equivalence classes of $\sim$, $< P \subset M >$ rather than the pairs $(P \subset M)$.

The neighborhood equivalence class of $< P \subset M >$ is denoted by $[P \subset M]$. The neighborhood equivalence class of a graph $(G \subset S^3)$ is called a N-graph type.

Next, we give a few remarks.

Remark 5.1.1. *1. Let $(G \subset S^3)$ be a graph. Then $\mathrm{N}(G; S^3)$ is a 1-handlebody. Further, if $G \in K(n)$, then $\mathrm{N}(G; S^3)$ has n 1-handles.*

2. If $G_1.G_2 \in K$ are such that $(G_1 \subset S^3) \sim (G_2 \subset S^3)$, then $G_1, G_2 \in K(n)$ for some n.

3. Let $(H \subset S^3)$ be a 1-handlebody in S^3 Suppose G_1 and G_2 are spines of H. Then $(G_1 \subset S^3) \overset{N}{\sim} (G_2 \subset S^3)$.

Now, we look at special kinds of graphs, called n-leafed rose. It is defined as the quotient space of n unknots $(C_1, C_2, \ldots, c_n)$ and a star with $n+1$ vertices $(v, v_1, v_2, \ldots, v_n)$ (v is the center vertex) where for all $i \in \{1, 2, \ldots, n\}$, a point on C_i is identified with v_i. The following figure illustrates this construction.

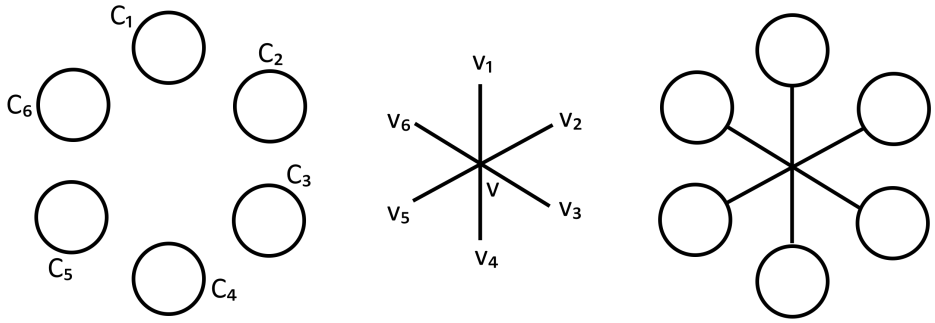

Figure 5.1: Illustration of construction of n-leafed rose.

The vertex v is called the base of the n-leafed rose.

Let $C(n)$ denote the subset of $K(n)$ whose elements are homeomorphic to n-leafed roses as described above. Define $C(0)$ to be $\{*\}$, where $*$ is a point. Let $C = \bigcup_{n\geq 0} C(n)$.

The proposition below follows from 5.1.1.

Proposition 5.1.2. *For any $[K \subset S^3]$, there is a n-leafed rose representative $< C \subset S^3 >$. Further, there are set identifications*

$$\{[G \subset S^3] \mid G \in K\} \longleftrightarrow \{[R \subset S^3] \mid R \in C\} \longleftrightarrow \{< T \subset S^3 > \mid T \in H\},$$

i. e., for $[G \subset S^3]$, you can find a representative $[R \subset S^3]$ where $R \in C$ and for $< T \subset S^3 >$, you can find a representative $[R \subset S^3]$ where $R \in C$.

Next, we define an operation on the sets $\{[G \subset S^3] \mid G \in K\}$ and $\{< T \subset S^3 > \mid T \in H\}$ using their representatives in $\{[R \subset S^3] \mid R \in C\}$.

First, for $\{< R \subset S^3 >\}$, we define $\vee$ as follows. Given $\theta_1 =< R_1 \subset S^3 >$ and $\theta_2 =< R_1 \subset S^3 >$ where $R_1, R_2 \in C$, we can represent them in a way that θ_1 in inside a S^2 and θ_2 is outside it and their base point coincides. We define $\theta_1 \vee \theta_2$ to be the $\sim$ equivalence class of the above structure. The following proposition captures the properties of the operation $\vee$.

Proposition 5.1.3. *Let $\theta_1 =< R_1 \subset S^3 >$ and $\theta_2 =< R_1 \subset S^3 >$ where $R_1, R_2 \in C$. Then $\theta_1 \vee \theta_2$ is well-defined. It is commutative and associative. The element $< U \in S^3 >$ where $U \in C(0)$ is the identity element. Hence, the set $\{[R \subset S^3] \mid R \in C\}$ with the operation $\vee$ forms a monoid.*

Using Proposition 5.1.2, we can define similar operation $\vee$ on the sets $\{< G \subset S^3 > \mid G \in K\}$.

We can also define a operation on $\{[R \subset S^3] \mid R \in C\}$. Let $\tau = [R_1 \subset S^3]$ and $\tau = [R_1 \subset S^3]$ where $R_1, R_2 \in C$. Like we did last time, we can represent them in a way that τ_1 in inside a S^2 and τ_2 is outside it such that they intersect in a 3-ball containing both of their base. We define $\tau_1 \vee \tau_2$ to be the $\overset{\text{N}}{\sim}$ equivalence class of the above structure. This operation also is well defined, commutative and associative. $[U \subset S^3]$ where $U \in C(0)$ is the identity element.

Using Proposition 5.1.2, we can define similar operation $\vee$ on the sets $\{[G \subset S^3] \mid G \in K\}$ and $\{< T \subset S^3 > \mid T \in H\}$.

The following theorem states that factorization with respect to the operation $\vee$ is unique (check [22] for factorization in rings).

Theorem 5.1.4. *In the monoids*

$$\left(\{< G \subset S^3 > \mid G \in K\}, \vee\right),$$

$$\left(\{< T \subset S^3 > \mid T \in H\}, \vee\right),$$

factorization is unique.

The prime elements of these monoids are precisely knots. Knots are thought of as elements of $\{< R \subset S^3 > \mid R \in C(1)\}$ or $\{[R \subset S^3] \mid R \in C(1)\}$.

There is also a nice formula for the fundamental group of handlebodies. This is due to the following theorem.

Theorem 5.1.5. *Let τ be an element of $\{[G \subset S^3] \mid G \in K(n)\}$. Then there exists knots $\tau_1, \tau_2, \ldots, \tau_n$ in $(\{[G \subset S^3] \mid G \in K(n)\}, \vee)$ such that*

$$\tau = \tau_1 \vee \tau_2 \vee \cdots \vee \tau_n.$$

Then the fundamental group $\pi_1(S^3 \setminus \tau) = \pi_1(S^3 \setminus \tau_1) * \pi_1(S^3 \setminus \tau_2) * \cdots * \pi_1(S^3 \setminus \tau_n)$

5.1.3 Complements of handle-bodies in $\mathbb{R}^3$

In the previous section, we saw how one can approach the fundamental group of the complement of a handelbody. In this section, we look at the homology groups of the complement of a handlebody. Since homology is weaker than the fundamental group (it cannot distinguish between knots), we will see that it is easier to find. The idea to to use Lemma 1.6.5 which states that if two subspaces are homotopy equivalent, then their complements will have same homology groups. We find homology groups of complements of simple embeddings of handlebodies. From Lemma 1.6.5, it follows that the homology groups of all embeddings are

same. We begin with two simple examples, complement of a genus 1 and genus 2 handlebody in $\mathbb{R}^3$.

Example 6. *Let T be a genus 1 handlebody in $\mathbb{R}^3$, which is simply a solid torus as shown in the following figure.*

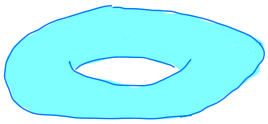

Figure 5.2: A torus in $\mathbb{R}^3$ whose complement we are interested in.

The complement of the torus in $\mathbb{R}^3$ then deformation retracts onto the wedge sum of a 2-sphere and a 1-sphere, i. e., $\mathbb{R}^3 \setminus T \approx S^1 \wedge S^2$. The following figure tries to show this.

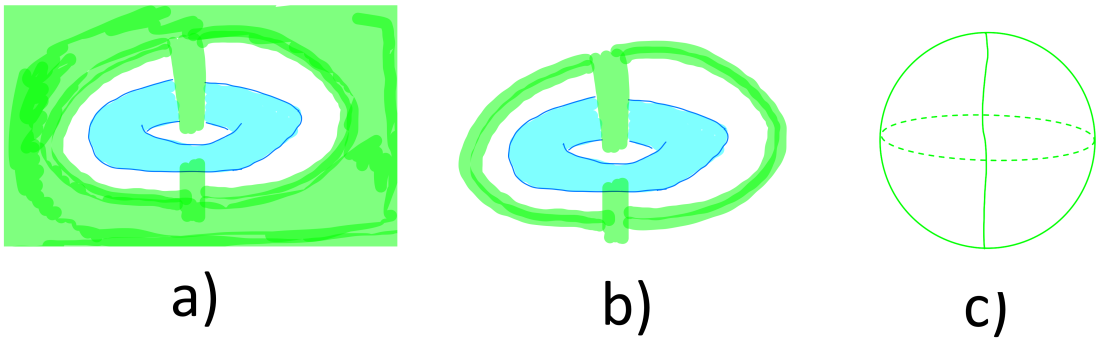

Figure 5.3: Attempt to visualize complement of a the torus in $\mathbb{R}^3$ in color green. a) Shows the torus along with its complement. It contains points going through the hole in the torus forming a rod and the points going to infinity outside it. b) The points going to infinity in the complement are compressed into a spherical shell. c) The spherical shell is further compressed into a 2-sphere and the rod into a line connecting with the 2-sphere.

Example 7. *Let S be a genus 2 handlebody in $\mathbb{R}^3$ as shown in the figure below.*

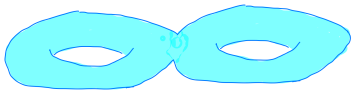

Figure 5.4: A genus 2 handlebody in $\mathbb{R}^3$ whose complement we are interested in.

The complement of S in $\mathbb{R}^3$ then deformation retracts onto the wedge sum of a 2-sphere and two 1-sphere, i. e., $\mathbb{R}^3 \setminus T \approx S^1 \wedge S^1 \wedge S^2$. The following figure tries to show this.

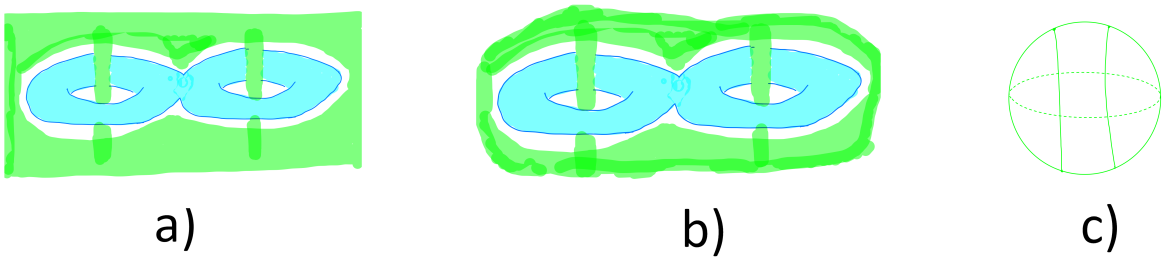

Figure 5.5: Attempt to visualize complement of S in $\mathbb{R}^3$ in color green. a) Shows the S along with its complement. It contains points going through the two holes in S forming two rods and the points going to infinity outside S. b) The points going to infinity in the complement are compressed into a spherical shell. c) The spherical shell is further compressed into a 2-sphere and the rods into a lines connecting with the 2-sphere.

In general, for a genus n 1-handlebody T_n embedded in $\mathbb{R}^3$ in a simple un-knotted manner, the argument given in the above examples generalize and we have

$$\mathbb{R}^3 \setminus T_n \approx \underbrace{S^1 \wedge S^1 \wedge \cdots \wedge S^1}_{\text{n times}} \wedge S^2$$

Now, using Lemma 1.6.5, complements of genus n 1-handlebody H embedded in any manner in $\mathbb{R}^3$ have the following homology groups.

$$\begin{aligned} \mathrm{H}_0\Big(\mathbb{R}^3 \setminus H\Big) &\cong \mathbb{Z} \\ \mathrm{H}_1\Big(\mathbb{R}^3 \setminus H\Big) &\cong \mathbb{Z}^n \\ \mathrm{H}_2\Big(\mathbb{R}^3 \setminus H\Big) &\cong \mathbb{Z} \end{aligned}$$

One can check that this is in accordance with Alexander duality for $\mathbb{R}^n$, Theorem 1.6.3, because $\mathrm{H}_0(H) \cong \mathbb{Z}$, $\mathrm{H}_1(H) \cong \mathbb{Z}^n$ and $\mathrm{H}_2(H) \cong \{0\}$. It also follows from the Proposition 5.1.2 which says that any genus n 1-handlebody has a n-leafed rose representative. The generators of the first homology group correspond to cycles passing though the petals of the rose. Note that in general, the petals of the rose would be knotted but homology does not detect that.

5.1.4 Under what assumptions can we assume that the particle space is a handle-body?

Now that we have discussed nice theory about handlebodies in S^3, we try to apply it to granular materials. We aim to model the particle space as a 1-handlebody. This is a reasonable assumption if all the particles intersect each other in disks. An example where two particles do not intersect in disks is given in the figure below.

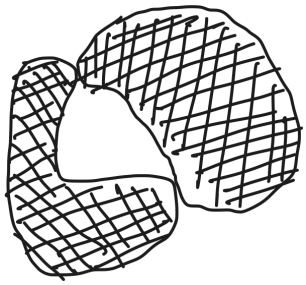

Figure 5.6: A 2D slice of two non-convex particles that do not intersect in a disk.

If the particles themselves are convex, then it is reasonable to assume that they intersect in disks.

5.1.5 Application to granular materials

We do not have a concrete application to granular materials in mind. We believe this is something to be explored. It feels natural that the knotting and linking in the particle space should physically manifest itself. For example, [14] discusses collections of highly non-convex particles like staples, etc and studies percolation in them. Hopf link formation is directly tied to the rigidity of the material. This is a topic to be explored further.

5.2 Dual Blocks, Cohomology and Complements

In this section, we briefly discuss some basic results about dual block decomposition of a polyhedron (a space that is the geometric realization of a simplicial complex) and how it

relates to taking complements of a subspace inside the polyhedron. The main reference for this section is [20].

The main motivation for exploring dual blocks was the following. If you have a graph in $\mathbb{R}^3$ and you want to look at the homology of its complement, it seems that the lines normal to the smallest cycles in the graph can be joined together to create loops in the complement. This was inspired from [25] where they use these smallest cycles in the contact network to find 1D ridges of the medial axis. We start with some definitions next.

5.2.1 Introduction to dual blocks and their relation with complements

Given a finite simplicial complex X, we first need its *Baryceneric subdivision* denoted by SdX. The vertices of SdX are the barycenters of simplices in X, which is the centroid of the simplex or the average of coordinates of its vertices. The barycenter of σ is denoted by $\widehat{\sigma}$. Barycenters of small simplices are described in the following figure.

Figure 5.7: Barycenters (green) for a 0-simplex, 1-simplex and a 2-simplex

A *flag* is a chain of simplices in X: $\sigma_{i_1} \subset \sigma_{i_2} \subset \cdots \subset \sigma_{i_k}$ for $k \geq 1$.

The faces of SdX are in one-to-one correspondence with flags:

$$\{\widehat{\sigma_{i_1}}\widehat{\sigma_{i_2}} \cdots \widehat{\sigma_{i_k}} \mid \sigma_{i_1} \subset \sigma_{i_2} \subset \cdots \subset \sigma_{i_k}\}.$$

A flag starting with σ can be thought of as a normal direction to σ. The dual block of a simplex σ, denoted by $D(\sigma)$ are the union of all simplices in SdX which correspond to flags

starting with σ. Formally,

$$D(\sigma) = \bigcup \{\widehat{\sigma_{i_1}}\widehat{\sigma_{i_2}} \cdots \widehat{\sigma_{i_k}} \mid \sigma = \sigma_{i_1} \subset \sigma_{i_2} \subset \cdots \subset \sigma_{i_k}\}$$

Dual block of a simplex, informally speaking, is kind of orthogonal to it.

For nice polyhedra, we have the following nice properties of dual blocks.

Lemma 5.2.1. *Let X be a finite simplicial complex that consists entirely of n-simplices and their faces. Let σ be a k-simplex of X. Then*

1. *The dual blocks are disjoint and their union is $|X|$.*
2. *The closure of $D(\sigma)$ is the geometric realization of a sub-complex of $\mathrm{Sd}X$.*
3. *The interior of $D(\sigma)$ is the union of all blocks $D(\tau)$ for which τ is a proper co-face of σ.*

There is a way to give orientation to the dual blocks and define boundary operation on that map a $D(\sigma)$ for a k-simplex σ to a sum of dual blocks $D(\tau)$ with $\sigma \subset \tau$. This leads one to naturally consider a chain complex built from dual blocks and the boundary operation. There is a very nice thing about this complex. Let σ, τ be a k-simplices of X, then $D(\sigma) \cap \tau = \emptyset$ if and only if $\sigma \neq \tau$ and $D(\sigma) \cap \sigma = \widehat{\sigma}$.

Remark 5.2.1. *The amazing consequence of this is that the dual block complex is isomorphic to the cochain complex used to define cohomology of X. The isomorphism is given by mapping the cochains $\sigma^* : X \to \mathbb{Z}, \sigma^*(\tau) = 0$ if $\sigma \neq \tau$ and $\sigma^*(\sigma) = 1$ to the dual block of σ, $D(\sigma)$. Further, the homology groups of the dual block complex are same as the homology groups of the simplicial complex X. This naturally leads to Poincaré duality.*

Next we present the result most relevant for us which connects dual blocks with complements.

Theorem 5.2.2. *Let X be a simplicial complex and let A be a sub-complex of X. Then $|X| \setminus |A|$ deformation retracts onto X^* where*

$$X^* = \bigcup_{\text{simplex } \sigma \in X \text{ such that } \sigma \notin A} D(\sigma)$$

A nice version of Lefschetz duality holds as a consequence of Theorem 5.2.2 and Remark 5.2.1 modulo orientation considerations. This is Theorem 70.2 in [20].

Theorem 5.2.3. . *Let (X, A) be a compact triangulated relative homology n-manifold. If (X, A) is orientable, then there are isomorphisms*

$$\mathrm{H}^{\mathrm{k}}(X, A) \cong \mathrm{H}_{\mathrm{n}-\mathrm{k}}(|X| \setminus |A|)$$

$$\mathrm{H}_{\mathrm{k}}(X, A) \cong \mathrm{H}^{\mathrm{n}-\mathrm{k}}(|X| \setminus |A|)$$

5.2.2 Application to granular materials

We do not have a concrete application of dual block decomposition for granular materials in mind. But we feel they can be useful for computation purposes. Since we work with CT scans of granular materials, the data can be represented on a simplicial complex X (homemorphic to $\mathbb{R}^3$). After segmentation, we would have the particle space as a sub-complex A of X. We can then use Theorem 5.2.2 to find homotopy equivalent representative V' for the void space. The homology groups of V' can be computed using the dual blocks and boundary operation for dual blocks.

Chapter 6

Conclusion and Future Directions

In this thesis, we analyse granular materials from the lens of topology. We ignore the geometrical information present in the material such as the shape and size of particles, their orientation, etc. We start by discussing elegant topological pipelines [23] and [25] that are used to segment the particle space and the void space respectively from the CT data that is usually used to study them. We then give a simplified topological model for the particle space in Section 2.8.

Since the particle space and the void space as topological spaces that are complements of each other. Naturally, we want to see how complementary the information in particle space and void space is. The main tool we used in this direction is Alexander duality for $\mathbb{R}^n$ 1.6.3. We get the following results (3.1, 3.2) from its application to granular materials.

1. 2D materials
   (a) Isolated lumps of particles create void tunnels around them.
   (b) A necklace of particles bounds an isolated void, there is an additional connected component of the void space which is the unbounded compound of the void space.
2. 3D materials
   (a) Isolated lumps of particles create void shell around them.
   (b) A necklace of particles links with a tunnel in void space.

(c) A cavity creates a connected component of the void space. There is an additional connected component of the void space which is the unbounded compound of the void space.

Next, we explore the contact network of a granular material and use the first handshaking Lemma to relate the first Betti number of the particle space (or the void space since they have the same first Betti number due to Formulas 1.6) to the sum of coordination numbers of each particle and hence to the average coordination number of the material,

$$\beta_1(G) = n\left(\frac{\overline{d}}{2} - 1\right) + c,$$

where n is the total number of particles, $\overline{d}$ is the average coordination number, and c is the number of connected components in the particle space. This is useful in the context of granular materials because in some cases one has information about the average coordination number (for example, Appendix A in [2]).

Lastly, we explore two ideas that might be fruitful in the study of granular materials but is something to be further explored.

1. We explore the use of handlebodies as a candidate for the particle space (assuming it is connected). This model would be accurate when the particles are convex and rigid. In this case, one is naturally led to knots and links in the handlebody. It requires further work to see if these correlate with physical properties of the granular material.

2. We explore the application of dual block complex to model the void space. There is a nice result, Theorem 5.2.2 that relates the complement of a sub-complex in a given simplicial complex to the union of some of its dual blocks. The application of this theorem in the context of granular materials is not apparent as of now but remains a topic to be further explored.

Bibliography

[1] Ryan T. Armstrong et al. "Correspondence of max-flow to the absolute permeability of porous systems". In: *Phys. Rev. Fluids* 6 (5 May 2021), p. 054003. DOI: 10.1103/PhysRevFluids.6.054003. URL: https://link.aps.org/doi/10.1103/PhysRevFluids.6.054003.

[2] Adrian Baule et al. "Edwards statistical mechanics for jammed granular matter". In: *Rev. Mod. Phys.* 90 (1 Mar. 2018), p. 015006. DOI: 10.1103/RevModPhys.90.015006. URL: https://link.aps.org/doi/10.1103/RevModPhys.90.015006.

[3] Serge Beucher and Christian Lantuejoul. "Use of Watersheds in Contour Detection". In: *Proceedings of the Workshop on Image Processing: Real-Time Edge and Motion Detection, Rennes*. 1979. URL: http://cmm.ensmp.fr/~beucher/publi/watershed.pdf.

[4] Y.-C. Chang et al. "Medial Axis Transform (MAT) of General 2D Shapes and 3D Polyhedra for Engineering Applications". In: *Geometric Modelling: Theoretical and Computational Basis towards Advanced CAD Applications. IFIP TC5/WG5.2 Sixth International Workshop on Geometric Modelling December 7–9, 1998, Tokyo, Japan*. Ed. by Fumihiko Kimura. Boston, MA: Springer US, 2001, pp. 37–52. ISBN: 978-0-387-35490-3. DOI: 10.1007/978-0-387-35490-3_3. URL: https://doi.org/10.1007/978-0-387-35490-3_3.

[5] Pawel Dlotko. "Cubical complex". In: *GUDHI User and Reference Manual*. 3.11.0. GUDHI Editorial Board, 2025. URL: https://gudhi.inria.fr/doc/3.11.0/group__cubical__complex.html.

[6] Frederik J S Doerr and Alastair J Florence. "A micro-XRT image analysis and machine learning methodology for the characterisation of multi-particulate capsule formulations". In: *Int. J. Pharm. X* 2.100041 (Dec. 2020), p. 100041.

[7] Herbert Edelsbrunner and John L. Harer. *Computational Topology: An Introduction*. Vol. 69. Providence, Rhode Island: American Mathematical Society, 2010. ISBN: 978-0-8218-4925-5. DOI: 10.1090/mbk/069.

[8] Herbert Edelsbrunner et al. "Morse-smale complexes for piecewise linear 3-manifolds". In: *Proceedings of the Nineteenth Annual Symposium on Computational Geometry*. SCG '03. San Diego, California, USA: Association for Computing Machinery, 2003, pp. 361–370. ISBN: 1581136633. DOI: 10.1145/777792.777846. URL: https://doi.org/10.1145/777792.777846.

[9] J. Gostick et al. "PoreSpy: A Python Toolkit for Quantitative Analysis of Porous Media Images". In: *Journal of Open Source Software* 4.37 (2019), p. 1296. DOI: 10.21105/joss.01296.

[10] The Guardian. *Crowd crushes: how disasters like Itaewon happen, how can they be prevented, and the 'stampede' myth*. 2022. URL: https://www.theguardian.com/world/2022/nov/01/how-do-crowd-crushes-happen-stampede-myth-what-happened-in-the-seoul-itaewon-halloween-crush.

[11] Allen Hatcher. *Algebraic topology*. New York: Cambridge University Press, 2001.

[12] Lorenz Holzer et al. *Tortuosity and Microstructure Effects in Porous Media: Classical Theories, Empirical Data and Modern Methods*. Cham: Springer International Publishing, 2023. ISBN: 978-3-031-30477-4. DOI: 10.1007/978-3-031-30477-4.

[13] Johannes Kepler. *De Nive Sexangula*. First formulation of the Kepler sphere packing conjecture. Frankfurt am Main: Godefridi Tampach, 1611.

[14] Seongmin Kim, Daihui Wu, and Yilong Han. "Percolation transition in entangled granular networks". In: *Nature Communications* 16.1 (Dec. 2025), p. 11410. ISSN: 2041-1723. DOI: 10.1038/s41467-025-66228-3. URL: https://doi.org/10.1038/s41467-025-66228-3.

[15] L. Kondic et al. "Topology of force networks in compressed granular media". In: *Europhysics Letters* 97.5 (2012), p. 54001. DOI: 10.1209/0295-5075/97/54001.

[16] M. Kramár et al. "Quantifying force networks in particulate systems". In: *Physica D: Nonlinear Phenomena* 283 (2014), pp. 37–55. DOI: 10.1016/j.physd.2014.04.006.

[17] Yukio Matsumoto. *An Introduction to Morse Theory*. Trans. by Masahico Saito and Kiki Hudson. Vol. 208. Translations of Mathematical Monographs. Providence, Rhode Island: American Mathematical Society, 2002. ISBN: 978-0-8218-1022-4.

[18] N. N. Medvedev et al. “An algorithm for three-dimensional Voronoi S-network”. In: *Journal of Computational Chemistry* 27.14 (2006), pp. 1676–1692. DOI: https://doi.org/10.1002/jcc.20484. eprint: https://onlinelibrary.wiley.com/doi/pdf/10.1002/jcc.20484. URL: https://onlinelibrary.wiley.com/doi/abs/10.1002/jcc.20484.

[19] Sebastiano Cultrera di Montesano et al. “Chromatic alpha complexes”. In: *Foundations of Data Science* 8.0 (2026), pp. 30–62. DOI: 10.3934/fods.2025003. URL: https://www.aimsciences.org/article/id/67d7fc292b0ae97dd29cf50d.

[20] James R. Munkres. *Elements of Algebraic Topology*. Menlo Park, California: Addison-Wesley Publishing Company, 1984. ISBN: 978-0201627282.

[21] James R. Munkres. *Topology*. 2nd ed. Upper Saddle River, NJ: Prentice Hall, Inc., 2000. ISBN: 978-0-13-181629-9.

[22] C. Musili. *Introduction to Rings and Modules*. Elementary introduction to ring and module theory. New Delhi, India: Narosa Publishing House, 1992, p. 230. ISBN: 9788185198644.

[23] Karran Pandey et al. “Morse theory-based segmentation and fabric quantification of granular materials”. In: *Granular Matter* 24.1 (Dec. 2021), p. 27. ISSN: 1434-7636. DOI: 10.1007/s10035-021-01182-7. URL: https://doi.org/10.1007/s10035-021-01182-7.

[24] Matthias Rauter et al. “Granular porous landslide tsunami modelling – the 2014 Lake Askja flank collapse”. In: *Nature Communications* 13.1 (Feb. 2022), p. 678. ISSN: 2041-1723. DOI: 10.1038/s41467-022-28296-7. URL: https://doi.org/10.1038/s41467-022-28296-7.

[25] Lindsay Riley, Peter Cheng, and Tatiana Segura. “Identification and analysis of 3D pores in packed particulate materials”. In: *Nature Computational Science* 3.11 (Nov. 2023), pp. 975–992. ISSN: 2662-8457. DOI: 10.1038/s43588-023-00551-x. URL: https://doi.org/10.1038/s43588-023-00551-x.

[26] Vanessa Robins et al. “Percolating length scales from topological persistence analysis of micro-CT images of porous materials”. In: *Water Resources Research* 52.1 (2016), pp. 315–329. DOI: https://doi.org/10.1002/2015WR017937. eprint: https://agupubs.onlinelibrary.wiley.com/doi/pdf/10.1002/2015WR017937. URL: https://agupubs.onlinelibrary.wiley.com/doi/abs/10.1002/2015WR017937.

[27] Jennie von Seckendorff and Olaf Hinrichsen. "Review on the structure of random packed-beds". In: *The Canadian Journal of Chemical Engineering* 99.S1 (2021), S703–S733. DOI: https://doi.org/10.1002/cjce.23959. eprint: https://onlinelibrary.wiley.com/doi/pdf/10.1002/cjce.23959. URL: https://onlinelibrary.wiley.com/doi/abs/10.1002/cjce.23959.

[28] Nithin Shivashankar and Vijay Natarajan. "Parallel Computation of 3D Morse-Smale Complexes". In: *Computer Graphics Forum* 31.3pt1 (2012), pp. 965–974. DOI: https://doi.org/10.1111/j.1467-8659.2012.03089.x. eprint: https://onlinelibrary.wiley.com/doi/pdf/10.1111/j.1467-8659.2012.03089.x. URL: https://onlinelibrary.wiley.com/doi/abs/10.1111/j.1467-8659.2012.03089.x.

[29] Nithin Shivashankar et al. "Felix: A Topology Based Framework for Visual Exploration of Cosmic Filaments". In: *IEEE Transactions on Visualization and Computer Graphics* 22.6 (2016), pp. 1745–1759. DOI: 10.1109/TVCG.2015.2452919.

[30] Shin'ichi Suzuki. "On linear graphs in 3-sphere". In: *Osaka Journal of Mathematics* 7.2 (1970), pp. 375–396.

[31] Visualization, Department of Computer Science Graphics Lab, and Automation. *Computational Topology : Theory and Applications*. 2022. URL: https://www.youtube.com/playlist?list=PLD_EbzpO9CeaBr0UFp1T3BBQhN9LAOcj_.

[32] Wikipedia. *Morse theory*. URL: https://en.wikipedia.org/wiki/Morse_theory.

[33] Wikipedia. *Voronoi diagram*. URL: https://en.wikipedia.org/wiki/Voronoi_diagram (visited on 02/26/2026).

[34] D. R. Wilkinson and S. F. Edwards. "Spontaneous Interparticle Percolation". In: *Proceedings of the Royal Society of London. Series A, Mathematical and Physical Sciences* 381.1780 (1982), pp. 33–51. ISSN: 00804630. URL: http://www.jstor.org/stable/2397364 (visited on 02/27/2026).